

AN ASSESSMENT OF MAGNETIZATION EFFECTS ON HYDROGEN CRACKING FOR THICK WALLED PIPELINES

CONTENT

▪	INTRODUCTION	1
▪	OBJECTIVES	1
▪	LITERATURE AND BACKGROUND	2
▪	EXPERIMENTAL PLAN AND PROCEDURE	2
▪	CHAPTER 1 PIGGING ANALYSIS ON PIPELINE	
○	Pigging: Concept and History	5
○	Objectives of Pigging	6
○	Application of Pigging Operations	7
○	In-Line Inspection Techniques	8
▪	Geometry Technique	9
▪	Ultrasonic Technique	9
▪	Magnetic Flux Leakage (MFL) Technique	9
○	Magnetic Flux Leakage (MFL) Tools	10
▪	Drive or Pushing System	10
▪	Magnetic System	11
▪	Sensor System	11
▪	Recording System	12
▪	Power System	12
○	New Approaches on Pigging Operations	13
▪	CHAPTER 2 MAGNETISM AND MAGNETIC PHENOMENA IN STEEL	
○	Introduction	15
○	Magnetic Poles	16
○	Magnetic Moment and Magnetization	18
○	Magnetic Effect of Currents	20
○	Magnetism in Materials	21
▪	Diamagnetism	23
▪	Paramagnetism	23
▪	Ferromagnetism	23
○	Magnetization Curves and Hysteresis Loop	24
○	Ferromagnetism	26
○	Demagnetizing Field and Factor	27
○	Magnetic Circuit	29
○	Magnetic Measurements	30
○	Magnetic Materials	32
▪	Hard Magnetic Materials	33

▪	CHAPTER 3	MAGNETIC FLUX LEAKAGE TECHNIQUE IN PIPELINE PIGGING INSPECTION	
○		Introduction	36
○		Classification of Magnetic Inspection Techniques	36
○		Magnetic Parameters in Magnetic Inspection Techniques	37
○		Magnetic Flux Leakage	37
○		Inspection of Pipeline Using MFL Techniques	40
▪		High-Sensitivity MFL Technique	40
▪		Field Levels in Magnetic Flux Leakage	41
▪	CHAPTER 4	EFFECTS OF HYDROGEN IN PIPELINE STEELS	
○		Introduction	43
○		Solubility	43
○		Diffusivity	45
○		Trapping	46
○		Hydrogen Permeation	49
○		Sources of Hydrogen	50
○		Environmentally Induced Cracking – Hydrogen Damage	53
▪		Hydrogen Embrittlement	53
▪		Blistering, Hydrogen Attack, Metal Hydride Formation, Shatter Cracks, Flakes, Fisheyes, Micro-perforations, and Degradation in Flow Properties	54
○		Hydrogen Damage Mechanism	55
○		Hydrogen Damage in Steel	57
○		Hydrogen Damage in Pipeline	60
○		Hydrogen Embrittlement of cathodic Protected Steels	64
○		Hydrogen Effect on Magnetic Properties of Steel	65
▪	CHAPTER 5	EXPERIMENTAL PLAN AND PROCEDURE	
○		Introduction	70
○		Material Characterization	
▪		Tensile Test	70
▪		Microstructure and Chemical Composition	71
○		Devanathan-Stachurski Permeation Cell – Experimental Procedure	73
▪		Objectives	73
▪		Principle	73
▪		Apparatus and Test Environment	73
▪		Specimens	75
▪		Test Procedure	76
▪		Environmental Control and Monitoring	76
▪		Procedures for Analysis of Results	76
▪		Reporting	76

○ Barnacle Electrode Method – Experimental Procedure	77
▪ Objectives	77
▪ Principle	77
▪ Apparatus and Test Environment	77
▪ Specimens	78
▪ Test Procedure	78
▪ Calibration and Standardization	78
▪ Calculations and Interpretation of Results	78
▪ Reporting	79
▪ Initial Hydrogen Concentration Determination	79
○ Magentic Properties	81
▪ REFERENCES	83
▪ MILESTONE CHART	87

AN ASSESSMENT OF MAGNETIZATION EFFECTS ON HYDROGEN CRACKING FOR THICK WALLED PIPELINES

PROGRESS REPORT

1. INTRODUCTION

In the Beaufort Sea (Alaska), pipelines are designed conventionally to protect against thermal effects, ice mechanics, and environmental concerns. To satisfy this condition, generally, steel pipes are designed with thicker walls (commonly ¾" wall thickness) using higher steel grades such as API 5L Gr. X52 and X70 (grades covered by the American Petroleum Institute Specification 5L). Since the integrity of the pipelines is nowadays monitored using inspection apparatus that travel through the pipe, operating in the Beaufort Sea requires a high level of confidence and reliance on these inspection tools (intelligent pigging tools). The most valuable "In Line Inspection" instrument to assess metal loss corrosion is the *Magnetic Flux Leakage* (MFL) tool. This technique performs on principles of magnetizing the pipe wall and then detecting a local flux leakage caused by anomalies relative to change in pipe wall thickness due to corrosion.

Due to the thicker pipe wall, the amount of magnetization needed to use MFL tools in Beaufort Sea is significantly more than in areas of the Gulf of Mexico or Pacific Coast. Therefore, the exclusivity of this application includes the use of thicker, higher strength, cathodically protected steel pipes and more frequent inspection techniques using larger magnetization strengths. In consequence, these operational characteristics bring out some pertinent questions: does this increased magnetism and high frequency of usage of MFL tools lead to hydrogen effects with cathodically protected offshore steel pipelines that will be thick walled and of higher-grade steel? Does this effect lead to higher corrosion rates from the relatively reduced anode service life? If there is a potential of enhanced hydrogen cracking, what are the possible precautionary actions?

The Department of the Interior (D.O.I.) and the Department of Transportation (D.O.T.) of the United States of America currently sponsor this research project, which will evaluate how high strength magnetic fields produced during frequent pigging of pipeline steels affect on the hydrogen-induced cracking susceptibility of thick walled pipeline steels. The laboratory procedures and equipments required to elaborate this study will be developed, built, and operated by personal of both the Metallurgical and Material Engineering and Petroleum Engineering departments at Colorado School of Mines.

2. OBJECTIVES

The main objective of this research is to experimentally comprehend and describe the role of the application of high strength magnetic field during frequent pigging of pipeline steels on the hydrogen-induced cracking susceptibility. The research project will

quantitatively measure the increased hydrogen activity in the thick walled, high strength steels due to the magnetization and establish if the augmented level of diffusible hydrogen is deleterious to the strength of the pipes. If the remaining magnetism in steel pipes after pigging causes significant enhancement in hydrogen solubility at either the internal or the external surface of the pipe, it will be determined if this phenomenon will promote the initiation of hydrogen assisted cracking. If the hydrogen effect is determined to be deleterious, possible corrective actions will be assessed, such as modified cathodic protection system and/or use of demagnetization tools following pigging.

3. LITERATURE AND BACKGROUND

A thorough literature search has been conducted for this project; however, it is continue as the project progresses. This literature search has concentrated on pipeline inspection techniques, magnetism in pipeline pigging inspection, magnetic phenomena in steels, the effect of hydrogen in pipeline steels, and the effect of cathodic protection methods as provider of hydrogen on pipeline steel surfaces. Four different chapters (Chapter 1 to 4) were developed to describe these subjects (Attachment # 1).

4. EXPERIMENTAL PLAN AND PROCEDURE

The hydrogen concentration in a material has been experimentally measured using an electrochemical technique, which was developed by Devanathan and Stachurski for the “accurate measurement of the instantaneous rate of permeation of electrolytic hydrogen through a metal membrane.” This sensitive electrochemical method (*Devanathan cell*) requires that “a diffusion gradient exist within the metal membrane or foil by producing hydrogen on one side, such as by cathodic charging, and removing it on the other side by anodic polarization with a potentiostat.” The instantaneous rate of permeation is recordable by a plot of anodic current against time, and the diffusion coefficient constant, which represents the amount of movement (migration) of hydrogen atoms from one part to another of the steel lattice. This coefficient is calculated from the plot by a variety of methods such as: (a) time lag method, T_{lag} ; (b) rise time constant, t_0 ; (c) breakthrough time, t_b ; and (d) permeation rate, P .

On the other hand, a *barnacle electrode* cell was developed to measure the hydrogen activity (diffusion) as well, and is being utilized to correlate hydrogen concentrations with delay failure in high-strength steels. This technique employs only the extraction part of the *Devanathan cell*, assuming that hydrogen is previously homogeneously distributed all through the sample. The *barnacle electrode* method replaces the potentiostat of *Devanathan cell* by a nickel/nickel oxide electrode to act as a stable and non-polarizing electrode (cathode) that keeps zero hydrogen concentration at the extraction-side-surface of steel (anode) by oxidizing the exiting hydrogen atoms to water. Although the *barnacle electrode* was developed as a useful field tool to detect hydrogen concentration of components exposed to service environments, it will be used in this study to measure both the hydrogen concentration and transport simulating

pipeline service conditions. To calculate hydrogen diffusion coefficient the Fick's first law is applied, considering the typical barnacle electrode extraction curve for different hydrogen concentrations, i.e. anodic current versus extraction time.

To determine the nature and size of the magnetic effect on the hydrogen activity on pipeline steel a minor modification of *Devanathan-Stachurski hydrogen permeation cell* and *barnacle electrode* is required. A magnetic field is applied using a DC-magnetic coil around a nail that is placed close to the specimen to simulate the whole effect of the magnetic flux leakage tool, i.e. the peak magnetization during and remaining magnetization after pigging. The experimental plans as well as the experiment procedure have already been completed. Some hydrogen charging experiments have been run to establish the optimum charging time and the initial hydrogen concentration for determining the hydrogen diffusion in high-strength steels (Attachment # 2). A list of references is included at the end of this document (Attachment # 3) as well as the milestone chart (Attachment #4).

Attachment # 1

Literature and Background

CHAPTER 1

PIGGING ANALYSIS ON PIPELINE

1.1 Pigging: Concept and History

After the oil discovery in North America during the 19th century, the most efficient method until now devised for transporting fluids in the oil, gas and petrochemical industries is a pipeline. Even though the construction material of the first pipeline is not recorded, the first pigging operation took place during 1870's to remove the paraffin deposits that were produced inside a crude oil pipeline. These paraffin deposits reduced the internal diameter of the pipe affecting the oil transportation process efficiency. Another relevant recorded pigging operation goes back to 1904 when a pig was considered to discover a mechanical damage inside a 4-in steel gas line in Montana, which was under ground after a rock slide (PPSA, 1995).

The pigging tool, commonly known as pig, is defined as a device that moves through the inside of a pipeline like a free moving piston, sealing against the inside wall with a number of sealing elements for the purpose of cleaning, dimensioning, or inspecting (figure 1). This definition covers in excess of 500 different designs and types of pigs. Pigs get their name from the squealing, scraping, noise made by a pipe cleaner (pigging tool) traveled through the steel line (pipeline). It sounded like a "pig squeal" in accordance with a pipeline operator comment at the beginning of the 20th century.

Pipeline failures have heightened the awareness of transmission pipeline systems. The integrity of the pipelines is monitored using smart or intelligent pigging and requires careful planning and execution to increase pipeline lifetime and to obtain successful results as well as to maintain production and to avoid downtime due to blockages. This method of monitoring is becoming industrially common and extremely regulatory by international laws. These regulations require that internal inspections be performed using equipment which provides for the detection of corrosion, cracks, laminations, and changes in pipe wall thickness, etc. Such inspections shall be performed following start-up and the need for subsequent inspections evaluated annually based on the initial finding and in view of operational conditions and quality of the transported product (Nespeca and Hvending, 1988).

In accordance with a recent study, mechanical damage is the single largest cause of failures on gas transmission pipelines and a leading cause of failures on hazardous liquid pipelines. The mechanical damage usually occurs after a pipeline is constructed and is caused by excavation equipment, which deforms the shape of the pipe, scrapes away metal and coating, and changes the mechanical properties of the pipe. In this case, intelligent pigs play another important function.

Internal inspection devices are integral parts of every pipeline-monitoring program and the inspection operation by pigging is a rapidly maturing technology based on instrumented pigs. Advancements in electronics and computing technology make this

technique more useful and benefit (Muhlbauer, 1992). In 1987 was necessary to confirm the technical capability and commercial availability of a new “State of the Art” inspection tool for use in the Ekofisk-Emden 36-in. gas pipeline: magnetic flux inspection (Nespeca and Hvending, 1988). As propose of this work, inspection tools and magnetic flux inspection technique will be widely explained in further sections.

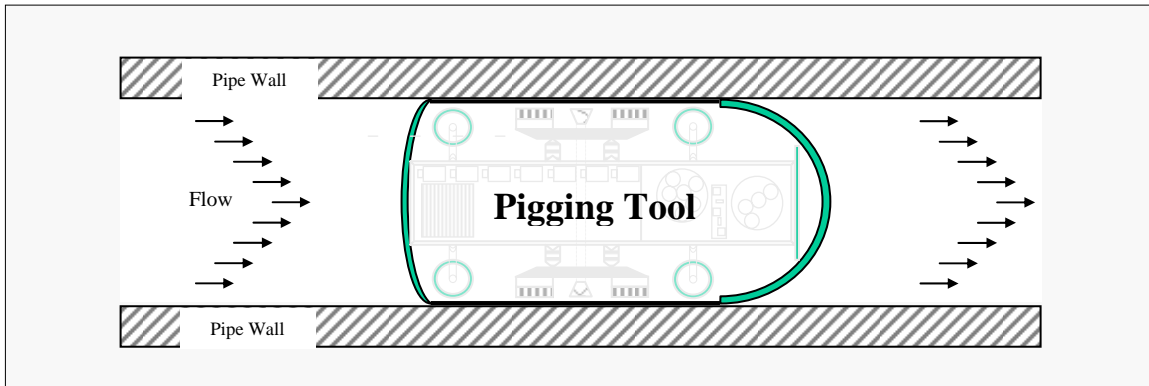


Figure 1. Common pigging tool “pig” used to clean, size or inspect pipelines.

1.2 Objectives of Pigging

Design a pipeline requires two fundamental concerns where pigs play a main function: continuous operation and investment efficiency. It means that pigging operation, which requires no interruption of pipeline services, must be economically profitable. The contribution of pigging inspection to guarantee nonstop functionality and maximum efficiency of the pipeline is achieved by (PPSA, 1995; Choumar, 1996):

- a) Eliminating internal deposits,
- b) Monitoring the physical and operational conditions and verifying them against current services requirements,
- c) Evaluating external coating conditions,
- d) Avoiding the formation of corroded sections,
- e) Supplying opportune data concerning any arising or apparent problems as well as potential repairs,
- f) Gauging its internal bore, and
- g) Reducing possibilities to design statutory recurrent tests.

The full-length pipeline pigging operation is the main advantage of smart or intelligent pigs when inspection is the principal concern. It further serves as the foundation for a pro-active maintenance program to safeguard against the consequences of failures. From pipeline stability management standpoint intelligent pigs have become of a paramount importance in the current and well known management of pipeline integrity (Choumar, 1996). Although intelligent pigs had some limitations in the 1980's

such as concealment of defects near circumferential or longitudinal welds, indication of unidentified defects, inaccurate grading and penetration of defect (Herve, et. al., 1981), nowadays those have been left in the past.

The current concept of Pipeline Integrity Management widely used by oil and gas industry is applied basically to define procedures to reduce the billions of dollars spent on corrosion control of pipeline systems. An effective management program that engages in the integrity threats typically associated with pipeline systems can reduce the probability of failure. These threats include, but are not limited to, external corrosion, internal corrosion, mechanical damage, and environmental assisted cracking. Some methods for evaluating pipeline integrity are identified by ‘the liquid rule.’ Those methods are hydrostatic testing, in-line inspection (ILI), and other equivalent and proven technologies (Vieth, 2002).

Pigging operations are feasible when specially designed launching and receiving vessels to introduce pigs into the pipeline are available. These vessels consist of a quick opening closure for access, an oversized barrel, a reducer and a neck pipe for connection to the pipeline. In addition, temperature, pressure and flow velocity are critical variables to control during any pigging operation.

1.3 Application of Pigging Operations

Although pigging operation was only used for removing liquid or solid deposits in the first years of oil and gas industry, nowadays it is involved in all pipeline life stages. Those basic phases essentially are construction, operation, inspection, maintenance, rehabilitation, and decommissioning of the pipeline.

- 1.3.1 *Pipeline construction* is the phase where pigs may be utilized to (a) remove metal remains, sand, stones, welding rods, rags and, sometimes, animals from inside the pipe. The pigging tool used is known as “debris-removal pig”. (b) Remove more stubborn debris from the pipe wall (mill scale, weld bead, etc.) using a cleaning or wire-brush pig. A dirty or choked down pipe produces a turbulent flow inside the pipeline, which becomes laminar after the cleaning process. (c) Ensure uniform internal diameter, i.e. without protruding inside the pipe. This initial gauging is made using a gauging pig. (d) Provide a whole record of data on the entire pipeline. The most useful information is number of joints, changes in inside diameter, exact location of any joint or internal protuberance, and if the valves of the pipeline system are completely opened. A geometry pig is running in this operation. (e) Remove air in front of hydrotest-fill water during hydrostatic testing.
- 1.3.1 *Pipeline operation* stage may require pigs to (a) Remove solid materials such as wax and scale to protect both the investment and the operational efficiency of the pipeline system. In this sub-stage “debris-removal pigs” can be used as well. (b) Ensure condensate is completely removed because

condensate dropout affects the effective bore of the pipe and erosion problems are present when turbulence exists. (c) Separate different substances that are transported through a multi-product pipeline using “batching pigs.” (d) Reduce the possibility of any contamination in a two-product interface by a batch of inhibitor run between two pigs.

- 1.3.3 *Pipeline inspection* or in-line inspection (ILI) operations cover a widely range of inspection services, however, the two most common requirements are for geometry measurement and metal-loss detection (PPSA, 1995). The pigging tools employed in pipeline inspection based on metal loss detection and sizing accuracy essentially are divided into two groups: ultrasonic and magnetic flux leakage tools. Any tool is technically good as long as it is used within specification and that its capabilities and limitations are identified before hand and meets the purpose of the exercise (Choumar, 1996). These two groups will be extensively described in next sections.
- 1.3.2 *Pipeline maintenance* and repair usually requires pigs to either clean or isolate specific section of the pipeline system. Cleaning pigs are run before in-line inspection operations to optimize inspection performance, while two conventional or utility pigs can be located in both ends of a specific section to isolate it from the entire pipeline to successful repair or modification.
- 1.3.3 *Pipeline rehabilitation* stage of the pipeline requires pigs to (a) apply chemical cleaning to remove stubborn substances. (b) Apply internal coating or clean the inside surface prior to the coating application itself. (c) Remove deposits of paraffin, asphaltene, or sediments by the proper use of suitable-aggressive cleaning pigs.
- 1.3.5 *Pipeline decommissioning* stage refers to methods and requirements for abandonment of pipelines. If the line is to be abandoned it might be cleaned and inspected before it is finally deserted. The pigs used to remove products, clean internally the pipe, and inspect it for internal and external damage are similar to those utilize in previous pipeline phases.

1.4 In-Line Inspection Techniques

Pipeline operators use a wide variety of methods to evaluate, inspect, and monitor the transmission pipelines now in operation worldwide, such as cathodic protection surveys, leak detection programs, excavations to look for pipe corrosion or protective coating failures, hydrostatic tests, and the use of in-line inspection tools that travel through the pipe (Nestleroth and Bubenik, 1999). As propose of this work, in-line inspection will be considered as the most relevant method of pipeline assessment.

For all intents and purposes, pumping a “smart electronic inspection pig” through the pipeline from one compressor station to the next performs in-line inspection. The use of pigs for in-line inspection of pipelines has increased considerably. The early years of

the 1960s was the beginning of in-line inspection with the introduction of a tool for corrosion measurement based on magnetic flux leakage technology. In 1980 a high-resolution magnetic flux leakage tool was developed starting a new era of in-line inspection tools. The geometry measurement pigs followed it using electro-mechanical devices (PPSA, 1995).

The primary use of the results from an in-line inspection using intelligent or smart pigging is not restricted to find out the health of the pipeline, but to calculate the maximum allowable operating pressure (MAOP) at which the pipeline can still safely be operated. In other words, determine acceptable anomaly or defect dimension before they become critical.

An in-line inspection program consists of the following components (Vieth, 2002): (a) system assessment/risk assessment, (b) identifying in-line inspection technology, (c) developing in-line inspection technical specifications, (d) investigative pig procedures, (e) quality assurance/quality control of in-line inspection results, and (f) in-line inspection verification.

Some of the nowadays available in-line inspection techniques upon which intelligent pigs are based on: geometry or caliper/deformation technique to characterize bend radii, dents and changes in ovality, ultrasonic and magnetic flux leakage techniques to characterize corrosion-caused metal loss and sizing.

1.4.1 Geometry Technique

This technique utilizes an electromechanical tool to inspect the geometric conditions of pipeline characterizing bends, dents, ovalities, sharp discontinuities and any mechanical deviation which distorts the cross section of the pipe. Although the physical damage may not cause the immediate rupture of pipeline (indeed it rarely does), this ‘insidious defect’ must be cautiously inspected. Geometry tools have been developed and improved continuously, and most now contain an electronic package and rely on computer analysis, which greatly enhances both the accuracy and the amount of information that can be provided (PPSA, 1995).

1.4.2 Ultrasonic Technique

The ultrasonic technique is based on measuring the ultrasound wave at internal and external pipe surface. The ultrasonic tool is the most accurate and suitable for corrosion monitoring/defect sizing but more difficult to handle and more expensive in comparison with magnetic flux leakage tools.

1.4.3 Magnetic Flux Leakage (MFL) Technique.

The magnetic flux leakage technique performs on principle of magnetizing the pipe wall using huge magnets and then detecting a local flux leakage caused

by metal loss (or gain) or other anomaly relative to change in pipe wall thickness. This technique can only be applied on ferromagnetic materials, such as low-alloy-carbon steels, which have a high magnetic permeability. The MFL tools are the most commonly used in-line inspection pigs and they may be run in oil, gas or a multiphase flow system.

1.5 Magnetic Flux Leakage (MFL) Tools

Magnetic flux leakage tools can be either segmented, with two or more parts joined by flexible connectors, or single piece, where all components are contained in a single, rigid package. Generally, segmented and single-piece MFL pigs incorporate several arrangements: drive or pushing system, magnetic system, sensor system (many rows of sensors covering the complete circumference of the pipe wall), data conditioning and recording system, and power system (figure 2). MFL tools generally require specially designed launching, running, retrieving procedures to introduce into, operate and remove the pigs from the pipeline. The fundamentals of launching, running and retrieving can be found in any pigging textbook.

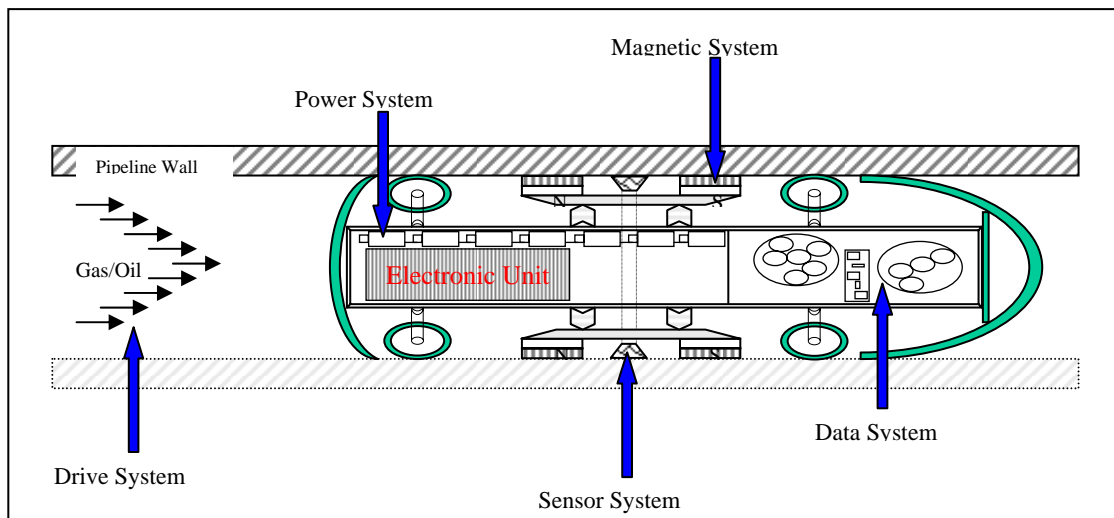


Figure 2. General systems incorporated in segmented or single-piece MFL pigs.

1.5.1 Drive or Pushing System

The force exerted by gas pushing on a cup or set of cups at the front of the tool pulls the tool through the line. The rear cups tend to have bypass holes to limit the pushing force. Differential pressure acting between the front and back of the drive cups provides a force along the pipe axis. This force propels the drive cups, which in turn pull the rest of the tool (Porter, 1996).

1.5.2 Magnetic System

The magnetic system is constituted by a set of magnets (either permanent magnets or battery-powered electromagnets) that are circumferentially arranged around the internal surface of the pipe and magnetize a length of its wall. The magnets make the transmission of the magnetic field to the pipe and its ends are connected to metal brushes placed against the pipe wall (Fig. 3).

Electromagnets produce a magnetic field by passing a current through a coil of wire, while permanent magnets have a homogeneous charge without external power to operate. It represents the most valuable advantage of permanent magnets and makes them the most commonly magnets used in modern MFL tools.

Particularly, the magnetic system of MFL tools is comprised of several high-strength rare-earth permanent magnets. Rare-earth magnets include Samarium-Cobalt (Sm-Co) magnets and sintered Neodymium-Iron-Boron (Nd-Fe-B) magnet. The measure of the magnet's force of attraction is called magnet's strength and it is categorized by a distinguishing characteristic known as Maximum Energy Product (BH_{max}). Nd-Fe-B magnets have a higher BH_{max} than Sm-Co magnets, which causes that Nd-Fe-B magnets are the most commonly magnets used in pipeline inspection industry. They Maximum Energy Product can easily reach 30 megagauss-oersted ($MGOe$) and even goes up to 50 $MGOe$ (MMC, 2001). Varying the number of magnets could change the strength of the magnetic system.

1.5.3 Sensor System

The sensor system is constituted by a set of sensor that records the leakage field during pipeline inspection. The leakage is transformed into a signal that is considered as a possible defect and can be later easily analyzed. The most common type of sensors used in MFL tools are induction coils (measure the proportion of change of a magnetic field) and Hall elements (more commonly used because they are not sensitive to tool speed, measure the current magnetic field strength).

The sensor size represents an important parameter because it directly impacts the resolution of the measurement system. All sensors have a length, width, and height and they provide an average measurement of the leakage field passing through the volume of the sensor (Porter, 1996).

1.5.4 Recording System

The signals recorded by the sensor system are processed by the data conditioning and recording system for later playback and analysis. New MFL-tool developments have digital recording systems, built on high-density computer tape storage technology, which provide data in a format suitable for use in computerized analysis systems.

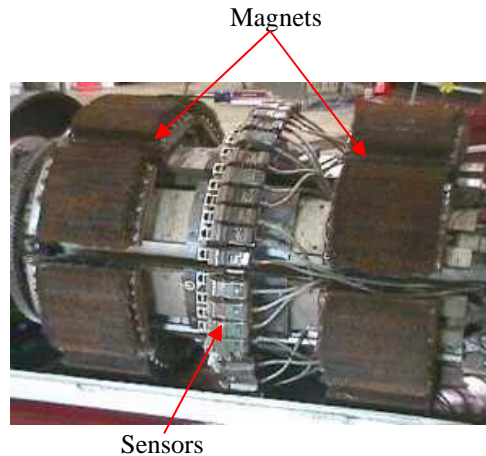


Figure 3. Typical magnetic (a) and sensor system (b) in MFL pigs (Nestleroth and Bubenik, 1999).

1.5.5 Power System

The data conditioning and data storage devices that are used in an MFL tool require power to operate, as well as some sensors. Therefore, the battery power that is available limits the mileage that can be inspected at any time. Most tools use rechargeable battery systems; the capacity of these systems and the energy requirements for the operating systems define the maximum inspection length (Nestleroth and Bubenik, 1999).

The measurements obtained from a MFL tool provide information regarding the physical condition of the pipeline (Bhatia and Westwood, 2003). These results are qualitative based on volumetric measurements, and its response to pipeline anomalies depends primarily on the magnetic properties of pipeline steel (permeability, etc) and the anomaly geometry itself. It is well known that material loss reduces the local ability of the pipe to carry magnetic flux, while plastic deformation (anomaly) due to mechanical damage locally changes the magnetic properties of steel (Bickerstaff, et. al., 2002).

Heavy wall pipelines present distinctive problems to pipeline inspection operations ranging from the magnetic requirements needed to saturate the pipe wall to the mechanical restraints of tool passage restrictions in

the pipeline. Typically, the design of MFL tools is compromise between the conflicting magnetic, mechanical, and electronic requirements (Bhatia and Westwood, 2003). MFL inspection of a pipe where the magnetic field does not saturate the pipe wall will be blind to external defects and will not be as sensitive to internal defect as a normal inspection.

The most important limitations of a MFL tool are based on its product flow restriction, the need for large quantities of data that is typically interpreted by humans, and the permanent magnetization left in the pipe steel after pig running. On the other hand, the MFL tool benefits are the accuracy of the test-true comparison obtained date and that it is capable to chose the level of sensibility according to testing needs: low, middle, high, extra high or newest extra high resolution tools (Nestleroth and Bubenik, 1999; Bickerstaff, et. al., 2002).

The *1st Generation Tools-Conventional/Low Resolution tools* report internal and external metal loss in bands (in order of magnitude), with no discrimination and no sizing. These tools are incapable of accurately assessing against specific pressure requirements. On the other hand, the *Mid-Resolution tools* are capable to discriminate between internal and external anomalies and to produce pressure-based reports.

The *High-Resolution tools* have the highest accuracy due to increased number of sensors, channels, and magnetic levels. While the *extra high* and *newest extra high generations* significantly increase the quality and number of small sensors to provide better anomaly sizing and higher resolution. The newest generation includes both inspection directions: circumferential and transversal.

1.6 New Approaches on Pigging Operations

In-line inspection is a pipeline-integrity verification method used to identify and characterize metal loss, deformation, crack-like features, pipeline movement, and positioning by use of a nondestructive testing tool traveling inside the pipeline. Different in-line pipeline inspection technologies are available to the operator depending of the treat of the integrity treat being evaluated. Pipelines operators are playing a key role in determining the pipeline industry's needs in conjunction with in-line inspection industry that continuously develops and improves its own capability to meet the challenges of better detection, sizing, and anomaly location (Vieth, et. al., 2002).

Over the last five years, many in-line inspection industry's companies have developed equipment to provide reliable inspection data for specific aspects of integrity. Technologies available cover a wide range of magnetic flux leakage (MFL) inspection systems. For example, a new external condition assessment tool was developed to

measure both external and internal corrosion and the wall thickness of pipeline using MFL technology. Another innovation is a new in-line rotating transverse MFL tool that detects axial cracks such as those caused by stress-corrosion cracking (Nye and Garrison, 2000).

Nye and Garrison (2000) point that nowadays MFL in-line inspection of small diameter and thick-wall pipelines is available by pigs that use sensors that do not need the voluminous shoes required for other MFL systems. Recently, a leader in-line inspection company developed a new tool which combines, in a single piece of equipment, variable-speed control, advanced multi-axis sensors, circumferential and axial MFL, high-resolution deformation, reduced MFL for mechanical damage detection and an inertial system for incorporation into a geographical information system.

Before recent in-line inspection innovations, old uncoated steel pipelines should be considered automatic candidates for replacement. In today industry, significant cost benefits can be realized by prolonging a pipeline life with a properly planned MFL inspection and replacement program. In 1999 was possible analyze corrosion on uncoated seamless steel pipelines even though irregular surfaces and variations of wall thickness makes difficult to grade the MFL inspection logs (mechanical defects, metal loss anomaly details and appurtenance locations). The irregular surface on the interior of seamless pipe produces sensor vibrations adding noise or clutter to the MFL signal plus the varying wall thickness makes it more difficult to properly saturate the pipe wall with the magnetic flux (Shamblin, 2000).

Narrow metal loss defects, such as pitting, in small diameter and thick wall pipelines are unavailable to be accurately detected by common MFL tools. In 1998, an intelligent pig applying magnetic measuring technique was found to be capable of detecting internal, localized type of corrosion defects in heavy wall pipes. The inspection pig was sensitive to internal local metal loss only. The in-line inspection program helped to determine the condition of several subsea flowlines in the central North Sea and to reduce potential failures (Van der Veer, et. al., 2000).

One of the most revolutionary developments was made in 2000 when was introduced the optimum multi-technology tool to inspect pipelines by MFL and to provide an inertial navigation and global positioning system (GPS). It reduces data collection from four different technologies to just two pigs run. In one direction, a pig checks internal wall geometry changes and gives a three dimensional (3-D) map of the line's position. In the reverse direction, another MFL tool detects corrosion defects distinguishing those, which are internal from external. Recent enhancements include varying magnetic levels to better check metal loss and physical damage, multi-axis sensors for better longitudinal anomaly length and width measurement (Staff Report, 2001).

CHAPTER 2

MAGNETISM AND MAGNETIC PHENOMENA IN STEEL

2.1 Introduction

The ancient Greeks and also the early Chinese knew about mysterious and rare stones with the unusual property to attract iron. A steel needle stroked with such a "lodestone" became "magnetic" as well, and around 1000 the Chinese found that such a needle, when freely suspended, pointed north-south.

The magnetic compass soon spread to Europe even when voyagers usually follow the stars. Columbus used it when he crossed the Atlantic Ocean, observing not only that the needle deviated slightly from exact north (as indicated by the stars) but also that the deviation changed during his voyages. Around 1600 the Englishman William Gilbert (1540-1603) suggested an explanation: "the Earth itself was a giant magnet, with its magnetic poles some distance away from its geographic ones". Gilbert's explanation eradicated many superstitions that had darkened the subject. No relevant magnetism discoveries were made for almost two centuries after Gilbert, although there were many improvements in iron-based magnet manufacturing.

Until 1821, only one kind of magnetism was known, the one produced by iron magnets. Then a Danish scientist, Hans Christian Oersted (1775-1851), while demonstrating to friends the flow of an electric current in a wire, realized that the current caused a nearby compass needle to move. It symbolized a great discovery: the first electromagnet. Andre-Marie Ampere (1800-1864) who studied this new phenomenon concluded that: "the nature of magnetism was quite different from what everyone had believed. It was basically a force between electric currents: two parallel currents in the same direction attract, in opposite directions repel."

Almost a century later Pierre Curie (1859-1906) introduced or clarified the ideas on diamagnetism, paramagnetism and ferromagnetism, and Paul Langévin (1872-1946) worked through induced and permanent magnetism. Pierre Weiss (1865-1940) made a relevant progress in his classical description of magnetism of solids, creator also of the molecular field hypotheses along with Louis Néel (1904-2000).

As propose of this work, permanent magnets will be widely mentioned. The modern history of permanent magnets commenced about 1940 with the introduction of AlNiCo (Alnico). Before this, the use of permanent magnets was limited to a few applications such as the compass and magneto. These are nowadays as well very function depended on the permanent magnetic properties. Electromagnets were replaced by permanent magnets after the introduction of Alnico, and the use of these magnets started to become widespread in devices such as motors, generators, loud-speakers, and inspection tools.

A major change in permanent magnetic materials industry started about 1970 with the introduction of the samarium-cobalt (SmCo) family of hard magnetic materials with magnetic energy densities hitherto undreamed of. This revolution accelerated recently with the discovery of a new generation of rare-earth magnets based on neodymium, iron and boron (Nd-Fe-B) with even higher magnetic energy densities than samarium-cobalt and with an anticipated lower cost. These two families of rare-earth magnets have such high energy densities that they can not only replace electromagnets, but also have applications not available to electromagnets (AMT, 2002). The discovery of strong Nd-Fe-B magnets was announced in 1983. Example of this useful magnet is in oil and gas pipeline inspection industry.

2.2 Magnetic Poles

The forces of attraction and repulsion between magnets, the most direct manifestation of magnetism, seem to start in regions located near their ends known as ‘poles.’ The end of a freely suspended magnet such as the needle of a compass that orients itself toward the geographic north pole of the earth is called ‘north pole.’ Hence opposite poles attract, and like poles repel, the geographic north pole is magnetically a south pole, and the geographic south pole is magnetically a north pole. Coulomb’s law (Charles Coulomb, 1736-1806) governs these magnetic forces of attraction and repulsion by analogy to electrostatics. Consider two poles with strengths of p_1 and p_2 , the forces between them is proportional to the product of those strengths and inversely proportional to the square of the distance among them (although the proportionality constant of Coulomb law is 10^{-7} , in this section it is assumed equal to 1):

$$F = \frac{p_1 p_2}{r^2} \quad (2.1)$$

Although it was usual in introductory texts of earlier days to postulate two types of magnetic poles separated by a distance, it is found that, no matter small the magnet is, north and south pole are inseparable (i.e. if a bar magnet is transversally cut in two separated pieces, new poles appear and two new magnets result). If such as an isolated pole was discovered, then, in analogy to electrostatics, it would become natural to postulate a force law of $1/r^2$ type, where the isolated pole would experience a central force. However, we see no isolated magnetic poles. We therefore say that no magnetic monopole has been hitherto discovered. We always see that a magnet manifests at least as a dipole. This means that the magnetic forces threaded by any closed surface is zero (Panat, 2003).

The magnetic field (lines of force) created around a magnetic pole by itself produces a force in the nearby pole, which is related to the pole strength (p_i) and the field strength or intensity (H). If a non-magnetized bar of iron is near a magnet, it will become magnetized. For this reason the field strength is also called the magnetizing force.

Assuming the proportionality constant equal to 1, the force acting on the magnetic pole is:

$$F = p H \quad (2.2)$$

In cgs system, the units of all variables shown in equations 2.1 and 2.2 are: F , dynes; d , centimeters; p , weber; and H , oersted (1 line of force/cm²). The magnetic field H is produced because of the orbital motions and spins of electrons within the magnet material that conduce to a magnetization within the material itself and the magnetic field outside.

Michael Faraday (1791-1867) represented the magnetic field with lines of force, which was considered later as a useful suggestion. Outside a magnet, the lines of force radiate outward from the north pole and return to the south pole (Fig. 2.1). It is possible to observe magnetic field lines in two dimensions with the aid of iron filings around a magnet, which after being magnetized are aligned parallel to the lines of force (Fig 2.2).

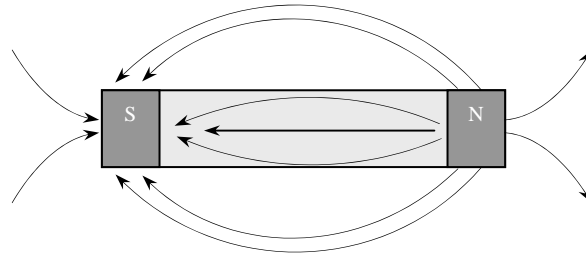


Figure 2.1. Lines of force in a common magnet representing a Magnetic Field.

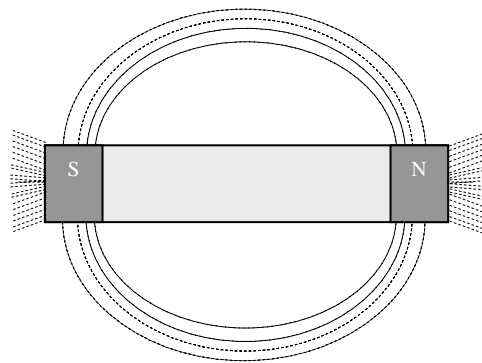


Figure 2.2. Magnetic field lines represented by sprinkling iron filings.

2.3 Magnetic Moment and Magnetization

The magnetic moment, an important and fundamental quantity applied to a bar magnet or to the electronic magnet, is considered the analogue of the angular momentum in mechanics. If a bar magnetic (dipole) of length l with poles of strength p and $-p$ at its ends, and it is suspended in the uniform magnetic field H , each pole is acted upon by a force that tends to turn it into the field direction. This means that a couple or torque is exerting on the magnet. From Fig. 2.3, the moment of the couple or torque is:

$$\Gamma = (p l) H \sin \theta \quad (2.3)$$

The product “ pl ” is the magnetic moment of the magnet, i.e. if the couple is acting on the magnet when it is at right angles (90°) to a uniform magnetic field of 1 Oersted, the magnetic moment (ergs/oersted) is given by:

$$m = p l \quad (2.4)$$

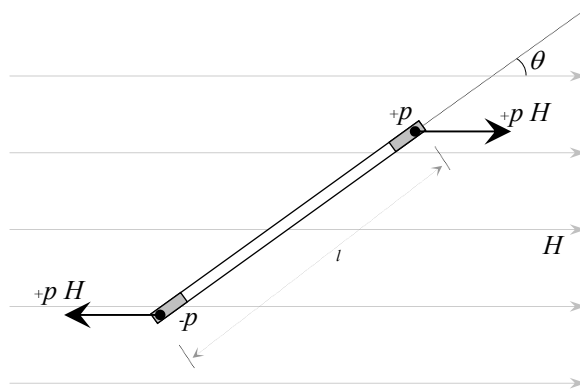


Figure 2.3. Suspended magnet in a uniform field under the action of a couple or torque.

Any kind of force acting on the magnet involves the pole strength p and the length l in the product pl . If no frictional forces act on the magnet, the work done by the torque in turning the bar magnet through a tiny angle $d\theta$ is reversible, originating a potential energy (E_p , ergs),

$$dE_p = (pH \sin \theta) (l) d\theta$$

In terms of the magnetic moment m and assuming that potential energy is equal to zero when the magnet is perpendicular to the field,

$$E_p = \int_{90^\circ}^{\theta} (m H \sin \theta) d\theta,$$

$$E_p = -m H \cos \theta \quad (2.5a)$$

Since the magnetic moment m and the magnetic field H are vectors, Eq. (2.5a) becomes

$$E_p = -\mathbf{m} \cdot \mathbf{H} \quad (2.5b)$$

When a magnetic material is subjected to a uniform magnetic field, it becomes magnetized; therefore the magnetic moment per unit volume is called magnetic polarization or intensity of magnetization. The intensity of magnetization or simply the magnetization, usually denoted by M , is a quantity extended of the magnitude to which the magnet are magnetized. Hence,

$$M = \frac{m}{V} \quad (2.6)$$

If in a unit volume of a magnetic material are several magnetic moments (m_1, m_2, \dots, m_i), the magnetization (ergs/oersted cm^3) is given by

$$M = \sum_{i=1}^n m_i \quad (2.7)$$

If the total number of magnetic moments (or dipole moments, n) is aligned parallel to each other and has the same magnitude (m), the magnetization, considering Eq. (2.4), is given by the new expression:

$$M = n p l \quad (2.8)$$

The magnetic pole density (ρ , Wb/m³) is the total quantity of magnetic poles occupying a unit volume of material and is commonly represented by the product 'np'. In addition, the surface pole density (ω) of a magnetic material is proportional to the magnetic pole density and the length of each magnet. Consequently, the magnetization can also be defined as the number of magnetic poles displaced across a unit cross-section because

$$M = npl = \rho l = \omega \quad (2.9)$$

2.4 Magnetic Effect of Currents

A magnetic field can be produced either by a permanent magnet (due to electrical motions and spins of electrons) or by a electrical charge in motion through a material. The magnetic effect of electric currents in conductors will be derived in this section for a complete understanding of the magnetism phenomena, however it is not the principal propose of this work.

The magnetic field H produced by an electrical current is calculated using the Biot-Savart law, which represent one of the fundamental laws of electromagnetism. A current flowing in a elementary length conductor (such as a straight wire) generates a magnetic field which geometry depends of the wire arrangement (Fig. 2.4) (Cullity, 1972).

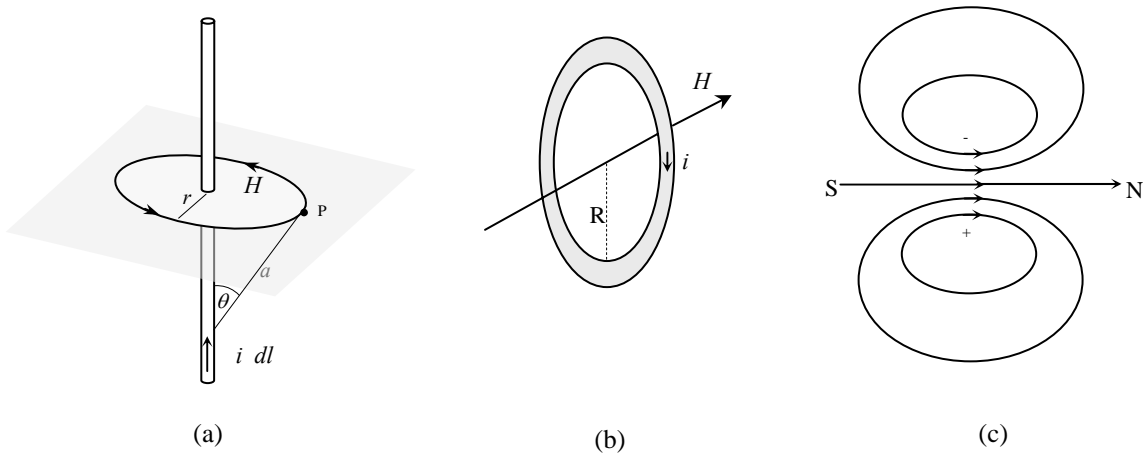


Figure 2.4. Magnetic fields due to an electrical current.

Bray and Stanley (1998) suggested that the general formula for the magnetic field H at some point P (r cm from the wire axis), due to a current (i) in an element of conductor dl (straight wire, Fig. 2.4 a) is given by

$$\mathbf{H} = \frac{i}{4\pi} \int_{\pi}^0 \frac{d\mathbf{l} \mathbf{a}}{a^2} \quad (2.10)$$

After some assumptions and considering cgs electromagnetic units (1 Oe = $10^3/4\pi$ A/m), the Eq. 2.10 becomes

$$H = \frac{2i}{10r} \text{ Oe} \quad (2.11)$$

The magnetic field intensity H on the center along the axis of a coil (Fig. 2.4 b) is

$$H = \frac{2\pi i}{10R} \text{ Oe} \quad (2.12)$$

The magnetic field of a single current loop is shown in Fig. 2.4 (c). Combining some current loops a more uniform magnetic field is produced. Since the solenoid is made by uniformly winding a few layers of wire on an elongated tube, the field along its axis is given by

$$H = \frac{1.257ni}{10L} \text{ Oe}, \quad (2.13)$$

where n is the number of turns that are wound evenly over the solenoid length L .

As the diameter of a current loop becomes smaller, the field of the loop (Fig. 2.4 c) approaches that of a magnetic dipole. Thus it is just as permissible to regard “a magnet as being a collection of current loops as a collection of dipoles”. In fact, André-Marie Ampère (1775-1836) suggested that the magnetism of a body was due to molecular currents circling in it, later called amperian currents. On a short section of a bar these current loops, called equivalent surface currents, would appear around it in the same direction. In consequence, it is impossible to describe all magnetic phenomena in terms of equivalent surface currents, without any reference to magnetic poles (Cullity, 1972).

2.5 Magnetism in Materials

The materials that are going to be considered in this work are ferromagnetic (such as almost all oil and gas steel pipeline materials), and how external magnetic fields interact with various kinds of substances will also be discussed. Useful and understandable examples of how may be measured the magnetic behavior of a substance is presented in some magnetism texts. However, Cullity (1972) considered the Rowland'

Ring as the circuit for magnetization (Fig. 2.5), which is a ring sample wound with two groups of wire-based windings (turns of isolated wire) connected to electrical components (switch, ammeter, and ballistic galvanometer). This configuration (toroid) has the advantage that the formation of magnetic poles is unnecessary to magnetize the ring material. Its principle is based on the comparison of the magnetic flux (Φ , weber) produced by the current flowing through the primary winding (calculated from Eq. 2.13) and the flux obtained from the galvanometer deflection (secondary winding).

When the ring contains any material substance the calculated magnetic flux is found to differ from that observed in the galvanometer. This difference is zero when the ring has nothing but empty space. According to the kind of magnetism that any material substance exhibit, those can be classify in: diamagnetic, paramagnetic or anti-ferromagnetic, and ferromagnetic or ferrimagnetic. The latter two groups are distinguished by magnetic measurements.

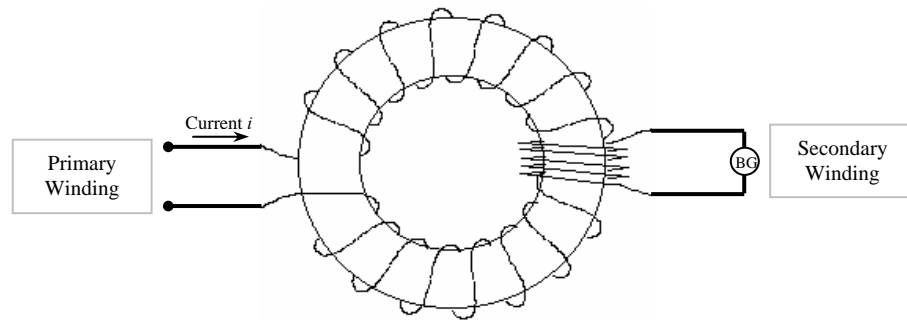


Figure 2.5. Circuit for Magnetization.

The internal mechanisms responsible for the observed magnetic behavior of various material substances are primarily related to the properties and nature of the electrons of the atoms of which every substance is formed. The electrons have their own magnetic moment due to their constant motions, orbital and spin, and the change in the orbital motion caused by any applied magnetic field. The sum of all electronic magnetic moments gives rise to the magnetic moment of the atom, which is an indispensable concept in the magnetism behavior of material.

Previous to describe the different kinds of magnetism and by which mechanism they are affected, let us define two essential concepts. (a) The presence of a magnetic field in a free environment will always cause the presence of a magnetic flux Φ , i.e., the flux is produced by the presence of a magnetic field in a medium. (b) The lines of force in a magnetized bar described in section 2.2 are applicable at macroscopic scale, however, in any internal section of a material small north-south poles are created by an external applied magnetic field H . These lines of magnetization added to the lines of forces constitute the lines of induction, and the total number of lines of induction per area unit is called the magnetic induction or total flux density B , which is proportional to magnetization M and magnetic field H . Generally, B is calculated from

$$B = \mu_o (M + H) \quad (2.14)$$

where μ_o is called the permeability of vacuum (fundamental physical constant), and has the value of $4\pi \times 10^{-7}$ henrys per meter (H/m).

2.5.1 Diamagnetism

Diamagnetism characterizes substances that have only non magnetic atoms: their magnetization, induced by the field, is very weak, and is opposite to the field direction (Du Trémolet et. al., 2002), i.e. atoms with electrons which constitute a closed shell in them and have their spin and orbital moments so oriented that the atoms as a whole has not net moment (Cullity, 1972). The mechanism by which the magnetization is induced opposite to the magnetic field is the acceleration of the orbital electrons by electromagnetic induction caused by the penetration of the magnetic field to the orbital (Chikazumi, 1997). This intrusive field causes a distortion in the inner electronic orbits and, in consequence, it causes small changes in electronic moment.

2.5.2 Paramagnetism

The own axial spins that the nuclei and atomic electrons in molecules have, besides orbital electron motion, causes orbital and spin moments, which are vectorially added to give the total moment. Bray and Stanley (1997) affirmed that paramagnetism result when these spins tend to align in the external magnetic field. However, spin orientations are randomized by temperature, so an average over all orientations must be found using Maxwell-Boltzmann statistics.

Paul Langévin (1872-1946) developed another theory of paramagnetism behavior. The Langévin theory of paramagnetism also leads to paramagnetic susceptibility that varies inversely with the temperature. It established that in materials with unpaired electrons, and consequently in which the orbital magnetic moments are not balanced, there is a permanent magnetic moment per atom.

2.5.3 Ferromagnetism

Some authors define ferromagnetic materials as paramagnetic substances with large molecular fields. However, there is not a single theory to explain the ferromagnetism behavior, but at least two rather divergent viewpoints: (a) the localized moment theory which declares that the electrons responsible for ferromagnetism are attached to the atoms and cannot move about in the crystal, and (b) the band theory, also called collective-electron theory and itinerant-electron theory, which affirms the electron responsible for ferromagnetism are considered to belong to the crystal as a whole and to be capable of motion from one atom to

another. As propose of this work, the ferromagnetism behavior, as the principal kind of magnetism exhibit by the most common pipeline materials, is widely discussed in further section.

2.6 Magnetization Curves and Hysteresis Loop

The magnetic properties of a substance are based in the magnitude and direction of the magnetization M as well as the way in which M varies with the applied field H . The ratio of these parameters is called the volume susceptibility (χ_v , emu/cm³ Oe):

$$\chi_v = \frac{M}{H} \quad (2.15)$$

From the physics standpoint, the variation of magnetization with the field is relevant because it transmits the concept of susceptibility and reveals the kind of material. On the other hand, engineering researches are usually involved in ferro- and ferrimagnetic substance investigations and the total flux density B produced by an applied field is the main concern. The ratio of B and H is called the permeability (μ), which in terms of Roland-ring experiment is given by the ratio of the obtained flux (galvanometer) and the flux produced by the current.

$$\mu = \frac{B}{H} \quad (2.16)$$

The most common way to represent the bulk magnetic properties of a substance is by a plot of M/H or B/H ratios that is called magnetization curve. Under usual circumstances the diamagnetic and paramagnetic materials have linear $M-H$ curves that do not reveal remaining magnetization once the field is removed. The magnetization curve of ferro- and ferrimagnetic materials is nonlinear. The magnetization M increases with increasing field until it reaches the magnetization saturation. At high magnitude of the magnetic field (H), M becomes constant at its saturation value of M_s (Fig. 2.6), which is dependent only on the magnitude of the atomic magnetic moments. Once the magnetic field is removed ($H = 0$), a remaining magnetization (remanence) is left and the irreversibility or hysteresis phenomena appears giving rise to hysteresis loop.

The suitability of ferromagnetic materials for applications is determined principally from characteristics shown by their hysteresis loops. Therefore materials for transformer applications need to have high permeability and low hysteresis losses because of the need for efficient conversion of electrical energy. Materials for electromagnets need to have low remanence and coercivity in order to ensure that the magnetization can easily be reduced to zero as needed. Permanent magnet materials need high remanence and coercivity in order to retain the magnetization as much as possible (Jiles, 1998).

Coercivity is the reverse magnetic field necessary to coerce the substance back to zero magnetic induction (Fig. 2.7).

The permeability of ferromagnetic materials declines unexpectedly and both coercivity and remanence become zero at the Curie temperature. All ferromagnetic substances become paramagnetic once a material is heated above its Curie temperature. For example, the transition temperature of iron, nickel, and cobalt are 770, 358, and 1131°C, respectively. The reason of the transition from ferromagnetic to paramagnetic will not be discussed in this work because this phenomenon does not occur in pipeline inspecting operations, but it may be obtained from many references.

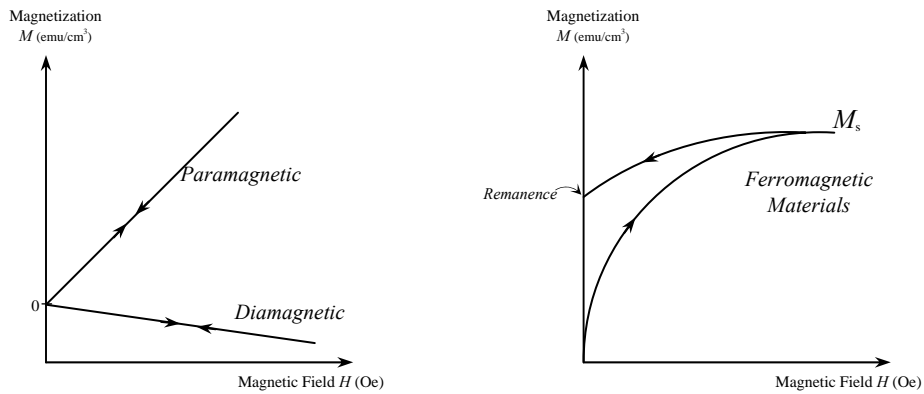


Figure 2.6. Typical magnetization curves of different substances.

Although a complete description of hysteresis loops may be found in any magnetism book, a briefly explanation of each loop stage is given in this section. From Fig. 2.7, once a magnetic field is applied (a) the substance follows a nonlinear magnetization curve until it reaches its magnetic saturation (b). When driving magnetic field drops to zero (c), the ferromagnetic material retains an appreciable degree of magnetization (remanence). Then, the magnetic field must be reversed and increase to a large value to drive the magnetization to zero again (d, coercivity). Thereafter the same amount of magnetic field force is slowly applied in the opposite direction toward the ‘magnetic saturation in the opposite direction’ (e). When driving magnetic field drops again to zero, due to the natural retentivity of the material, it will hold a magnetic flux with no magnetic field applied (f, remanence). Finally, the field is re-applied and the flux density reaches its prior value (b) passing first by another coercivity point (g).

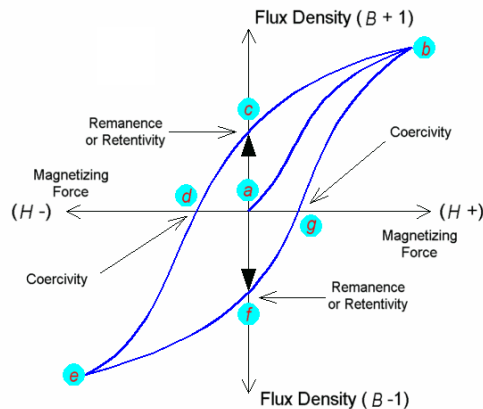


Figure 2.7. Hysteresis loop (from Learn Electronics Tutorials, <http://www.twysted-pair.com/hyster1.htm>).

In conclusion, the hysteresis loop shows the history dependent nature of magnetization of a ferromagnetic material. Once the material has been driven to saturation, the magnetizing field can then be dropped to zero and the material will retain most of its magnetization, i.e. it remembers its history (Nave, 2000).

2.7 Ferromagnetism

The term *ferromagnetism* is used to characterize strongly magnetic behavior, such as the strong attraction of a material to a permanent magnet. The origin of this strong magnetism is the presence, at the microscopic scale, and below the Curie temperature, of a spontaneous magnetization produced by a parallel alignment of spins. It means that all magnetic moments in a ferromagnetic substance are spontaneously parallel to each other (Chikazumi, 1997; Du Trémolet et. al., 2002). In 1907 Pierre Weiss explained the mechanism for the appearance of spontaneous magnetization, assuming that in a ferromagnetic substance exists an effective field called molecular field. This strong molecular field acts below as well as above the Curie temperature of each particular substance, and it could be magnetized to saturation by the molecular field even in the absence of an applied field. The substance is then self-saturating or spontaneously magnetized. The intensity of the molecular field (H_m) acting on a material is directly proportional to the saturation magnetization (M_s) by the molecular field coefficient γ , or

$$H_m = \gamma M_s \quad (2.17)$$

Iron and iron-based alloys (steel) are examples of self-saturating materials. Nevertheless, it is possible to obtain a piece of iron in the unmagnetized condition, and Weiss also explained why it is probable assuming that: ferromagnetic materials in unmagnetized conditions are divided into very some small regions known as *domains*. Two domains are separated by a boundary called *domain wall*. Every region or domain is impromptu magnetized to saturation, but the directions of magnetization of all regions are such that the total magnetization of the specimen as a whole is zero. This means that the domains have random orientations.

The average magnetization of a ferromagnetic material under an external field (H) and a molecular field (H_m) is given by

$$\left(\frac{m(H + H_m)}{kT} \right)$$

$$M = N m L \quad (2.18)$$

The solution of the Eq. 2.18 can be obtained graphically from the $M-\alpha$ plot (Fig. 2.9). The parameter α in this case is equal to $m (H+H_m)/kT$. The curve a represents the Langévin function and the straight-line b is the representation of the Eq. 2.18 when the external field is zero at a defined temperature T . The external magnetic field is not necessary to produce a spontaneous magnetization. Then, the intersection points of both curves represent solutions where O defines an unstable solution and P a stable one.

The spontaneous magnetization is a temperature dependence parameter, and lets consider it on the basis of the graphical solution. At $T=0$, the slope of line b is zero, $L(\alpha)$ is equal to 1, and $M=Nm$. It is known as the absolute saturation magnetization state. As the temperature increases to T_2 , the slope of the straight-line b increases as well and it rotates counterclockwise about the origin (Fig. 2.8–c). This rotation causes ‘ P ’ and its corresponding M value to move down along the Langévin curve (a) until it finally approaches ‘ O ’. The final reached temperature is known as the Curie temperature or Curie point. At any higher temperature, the spontaneous magnetization of a ferromagnetic material vanishes and it becomes paramagnetic.

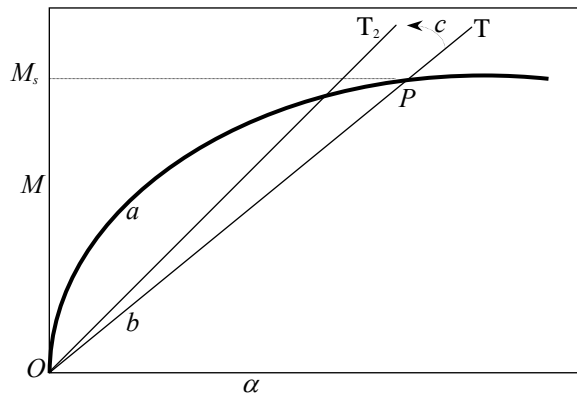


Figure 2.8. Graphical solution for spontaneous magnetization (a , Langévin curve).

2.8 Demagnetizing Field and Factor

In view of the fact that the presence of the magnetic dipole moment inside a magnetized material of finite size make that the free poles (which appear on its ends) produce a magnetic field directed opposite to the magnetization M produced by the external applied magnetic field H , it is possible to define a *demagnetizing field* (H_d) whenever poles are created in a material. The demagnetizing field depends on the

magnetization in the material and the shape of the specimen. This field is proportional to the magnetic free pole density and consequently to the magnetization. It is given by

$$H_d = N_d M \quad (2.19)$$

where N_d is called the *demagnetizing factor*, which is calculated solely from the specimen geometry (i.e. it is a large number for a thick and small sample and nearly zero for a elongated thin sample magnetized along its long axis).

Accurate analytical solutions for the demagnetizing factor N_d may be obtained in the case of second-order shapes (such as spheres and ellipsoids), and approximate solutions are accessible for solids of different geometries. For example, the demagnetizing factor (a dimensionless number) for a sphere is 1/3, for a cylinder magnetized perpendicular to its long axis is 1/2, and for a semi-infinite plate magnetized normal to its surface is 1.

In order to determine the exact internal field H_i in a solid of finite dimensions is necessary to make some demagnetizing field correction of the applied magnetic field H_a . The correction is due to it has been shown that the demagnetizing field arises in a specimen of finite shape with magnetization M in zero field.

$$H_i = H_a - N_d M \quad (2.20)$$

In terms of magnetic induction B , Eq. 2.20 becomes

$$H_i = \frac{H_a - N_d B / \mu_0}{1 - N_d} \quad (2.21)$$

The parameters susceptibility and permeability can also be corrected due to the effects of the demagnetizing field. If true (material property) and measured (dependent on geometry) susceptibility and permeability are defined as $\chi_{\text{true}} = M/H_i$, $\chi_{\text{meas}} = M/H_a$, $\mu_{\text{true}} = B/H_i$, and $\mu_{\text{meas}} = B/H_a$, the corrected χ and μ for demagnetizing factor are

$$\chi_{\text{true}} = \frac{\chi_{\text{meas}}}{1 - N_d \chi_{\text{meas}}} \quad (2.22)$$

and

$$\mu_{\text{true}} = \frac{\mu_{\text{meas}} - N_d / \mu_0}{1 - N_d} \quad (2.23)$$

2.9 Magnetic Circuit

The concept of magnetic circuit is important in the design of devices containing permanent magnets such as pipeline in-line inspection tools. In engineering applications of permanent magnets interruption of magnetic flux path by an air gap is commonly approachable alike metal loss defects in pipeline surface. Therefore, the complicated calculation of the magnetic flux in magnetic circuits with a combination of a ferromagnetic material (iron and iron-based alloys) and air is required. The air gap produced by any metal loss defect increases the reluctance (i.e. any ferromagnetic material is not placed in this area) of the magnetic circuit and reduces the magnetic flux in both the iron and the gap.

Assuming that an iron ring with permeability μ , average length of L and cross section of A is wound with n turns of a solenoid (which carries a current i). Then the magnetic flux (or flux density) passing in the ring can be calculated by Eq. 2.14. Sense $H=ni/L$ (from Ampère's law), the magnetomotive force (η) is defined as ' ni ', and the magnetic reluctance of the path (R_m) is equal to $L/\mu A$, a general equation to calculate the magnetic flux is defined as (proofs may be found in magnetism books)

$$\Phi = \frac{\eta}{R_m} \quad (2.24)$$

or

$$\Phi = \frac{ni}{L/\mu A} \quad (2.25)$$

The magnetic reluctance of the path is analogous to electrical resistance in an electric circuit, which means that magnetic reluctances in series in a magnetic circuit may be added. The equation for the flux passing through a toroid with an air gap is given by (Jiles, 1998)

$$\Phi = \frac{ni}{L_i/\mu_i A_i + L_a/\mu_a A_a} \quad (2.26)$$

where the subscripts represent the iron ring (i) and the air gap (a). In pipeline in-line inspection tools, the flux density in the pipe wall must be as high as possible in order to provide sensitivity to outer surface defects. Considering the core fluid inside the pipe (c), the air gap (a), and the iron-based pipe (i), the Eq. 2.38 becomes

$$ni$$

$$\Phi = \frac{1}{L_i/\mu_i A_i + L_c/\mu_c A_c + 2 t_a/A_a} \quad (2.27)$$

where t_a represents the distance between the magnets on the inner pipe surface (Bray and Stanley, 1997). The leakage of the magnetic flux due to any flaw is measured by sensors placed inside the inspection tools, which send the signals by telemetry (wireline) to the recording system. This procedure is known as ‘Magnetic Flux Leakage’ or MFL inspection technique, which will be widely described in further chapter.

2.10 Magnetic Measurement

Several methods to measure magnetic field, magnetic induction or magnetization are available and widely explained in magnetism books. Basically, these methods are nowadays divided into three principal categories: induction methods (based on magnetic induction measurement), force methods (based on measurement of force caused by magnetic field), methods based on changes in material properties due to magnetic field effects. The SQUID, largely utilized for ultra sensitive magnetometry, is a high-tech device that exploits quantum interference in superconducting junctions and is considered as part of another category of magnetic field measurement methodology that will not be include in this work.

Because pipeline MFL in-line inspection tools commonly use induction coils and Hall elements in their sensor systems to detect leakage of magnetic flux, these two groups (*induction methods*, that measure the rate of change of a magnetic field, and the *methods based on changes in material properties*, that measure the actual magnetic field strength) will be broadly describe in this section. The force-method group is based on the force on a magnetic dipole in a field and is constituted by four individual methods called torque magnetometer, force balance, alternating gradient force magnetometer, and the atomic force microscope.

The induction group of magnetic measurement methods is dependent on Faraday’s law of electromagnetic induction and is constituted by stationary-coil method, moving-coil method, rotating-coil method, vibrating-coil magnetometer, vibrating-sample magnetometer, and fluxgate magnetometer. A electromagnetic force (*emf*) in a coil is produced by any change respect to time in the magnetic flux (Φ) passing through the search coil (which is caused by any of he following reasons: removing the coil from the magnetic field, rotating the coil by 180° about an axis perpendicular to the field, reducing the intensity of the field, or reversing the sense of the field). From pipeline inspection standpoint (Nestleroth and Bubenik, 1999), the flux density is constant in a region with no imperfections. Therefore, no voltage will be induced when no defect is present. When an imperfection causes flux to leak into the air, a voltage is induced because the flux density is changing.

The fundamentals of induction coil methods declare that the electromagnetic force induced in a circuit formed by a coil with N turns is equal to the degree of change of flux linking the circuit,

$$emf = -N \frac{d\Phi}{dt} \quad (2.28)$$

In terms of magnetic induction B , and considering a coil with a cross-sectional area A , from the Faraday's law Eq. 2.28 becomes

$$emf = -NA \frac{dB}{dt} \quad (2.29)$$

The induced voltage is increased if B is increased while H is maintained constant by inserting a high-permeability core into the coil. In free space, $B = \mu_0 H$ and so (Jiles, 1998)

$$emf = -NA\mu_0 \frac{dH}{dt} \quad (2.30)$$

The voltage or electromagnetic force generated by a specific induction coil method (stationary-coil method, moving-coil, rotating-coil, vibrating-coil, vibrating-sample, and fluxgate) is calculated using Eq. 2.29 or its particular modifications.

The Hall effect took its name from Edwin Hall (1855-1938) who discovered in 1879 the effect of a perpendicular magnetic field on any conductor material carrying an electrical current (Fig. 2.9). When a transverse magnetic field (H) is applied to a plate-shaped conductor (metal or semiconductor), the current (i) that flows through it is distorted and an Hall electromagnetic force (emf_H) is produced between the two opposite points a and b , which had the same potential in the absence of the field. The magnitude of the emf_H is given by

$$emf_H = \frac{R_H i H}{t} \quad (2.31)$$

where t is thickness of the plate and R_H is the Hall constant. The material property R_H can be positive or negative as a function of charge carriers, and is determined by the interaction of the current with the material crystal lattice (typically 10^{-5} volt-cm/amp-oersted in semi-conductors). Commonly, commercial Hall elements are manufactured of InSb, InAs, or Ge.

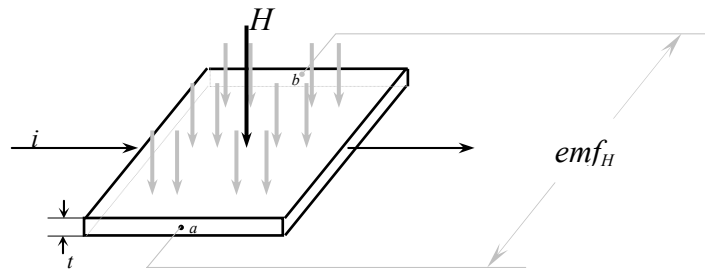


Figure 2.9. Relation between magnetic field, electrical current and the electromagnetic force (emf) in the Hall effect.

The Hall effect magnetometer (sensor) can be fabricated with very small active areas, down to 10^{-6} m^2 , which can therefore be used to measure the magnetic field with high spatial resolution. Another important factor is that unlike coils, which measure the flux linkage and therefore need to be scaled appropriately for their cross-sectional area in order to determine the magnetic induction, the Hall magnetometer measures the magnetic field strength directly (Jiles, 1998).

From pipeline inspection standpoint, newer Magnetic Flux Leakage inspection tools often use Hall elements. The most common type of Hall element used in MFL tools directly converts the magnetic field level to an output voltage, which is directly proportional to the flux density and is not dependent of the relative velocity with which the sensor passes through the magnetic field.

2.11 Magnetic Materials

Engineering applications of ferromagnetic materials are divided into three principal categories: (a) soft ferromagnetic materials, almost exclusively associated with electrical circuit (AC applications), (b) semi-hard magnetic materials, associated with magnetic recording purposes, and (c) hard ferromagnetic materials, associated with permanent magnets. The latter category will be extensively describe in this section because it is associated with the most common type of magnetic materials used in pipeline MFL inspection tools (permanent magnets).

However, it is important to mention that soft ferromagnetic materials find wide applications in consequence of their ability to improve the flux produced by an electrical current. The desirable properties for soft magnetic material to be used in electrical power generation and transmission applications such as the magnetic cores of transformers, motors or related devices, are high permeability, low coercivity, and low hysteresis loss. Because permeability indicates how much magnetic induction is generated by the material in a given magnetic field the higher the permeability the better for soft magnetic materials. Commonly a material with low coercivity (below 1000 A/m) is considered magnetically *soft*. Finally, since hysteresis loss represents the energy expended during one cycle of the hysteresis loop and for AC applications energy dissipation should be minimized, the hysteresis loss must be as low as possible (Jiles, 1998).

Most commonly used soft ferromagnetic materials for AC application are: silicon-iron alloys, iron-nickel alloys, iron-cobalt alloys, iron-cobalt-nickel alloys, iron-aluminum alloys, iron-carbon alloys, and amorphous magnetic alloys. Other substances such as *soft ferrites* are used in the soft magnetic materials industry.

2.12.0 Hard Magnetic Materials

Hard magnetic materials, or permanent magnets, are used to provide a magnetic field in a particular volume of space. The principal properties of these materials are their high coercivity field and high residual magnetization. For many engineering applications such as pipeline MFL inspections, permanent magnets are used because provide a constant magnetic field without the continuous consumption of electricity and without the generation of heat. The magnetic field is maintained due to the energy stored into the magnet when it was previously magnetized or ‘charged’, and it may remain in the magnet indefinitely. Therefore a high remanence is desirable and, in consequence, high saturation magnetization.

The quality of permanent magnet materials is determined by the maximum energy product $(BH)_{\max}$, which represent the maximum area under the magnetization curve in the second quadrant of the hysteresis loop (from the remanence to the coercivity point: *demagnetization curve*; Fig. 2.13a). For most efficient use of the magnetic material, the working point of the magnet should correspond to the maximum value of the energy product (Chikazumi, 1997). The energy of a magnet is always available for use and is not drained away by repeated use because a magnet does no net work on its surroundings (Cullity, 1972).

Considering the Ampere’s law in the magnetic circuit of a permanent magnet, where no current is flowing,

$$\oint_{\text{allspace}} H dl = 0 = \oint_{\text{inside magnet}} H dl + \oint_{\text{outside magnet}} H dl \quad (2.32)$$

Bray and Stanley point that Eq. 2.32, after some assumptions and considerations, becomes

$$B_{\text{inside magnet}} = - \left(L_m A_g / L_g A_m \right) \mu_o H_m \quad (2.33)$$

where L and A are represent length and cross-sectional area, and m and g refer to inside and outside the magnet. The Eq. 2.33 represents a straight line in the second quadrant that intersects the B-H curve at its operating point (Fig. 2.13b).

Since the desirable properties of permanent magnet materials are typically stated in terms of coercivity and remanence, they deserve some explanation. The coercivity is used to differentiate soft and hard magnetic material. High coercivity in a permanent magnet is desirable because it requires being highly resistant to demagnetization considering that it operates without an applied field.

Jiles (1998) points that the coercivity can be defined as either the field at which the magnetization is zero (intrinsic coercivity, mH_c) or the field at which the magnetic flux density in the material is zero, BH_c . These quantities have quite different values in hard magnetic materials, and the greater the difference the better the material is as a permanent magnet. High coercivity combined with high remanence is essential in hard magnetic materials. Since the remanence M_R is the maximum residual magnetization which can be obtained only in a closed-loop configuration and the residual magnetization at which the permanent magnet operates in open circuit is always below M_R , permanent magnets must be operated in an ‘open circuit’ configuration. The intrinsic coercivity in neodymium-iron-boron magnets is typically 1.12 MA/m while the remanence is typically 1.05 MA/m, which represent high values if are compared with other hard magnetic materials.

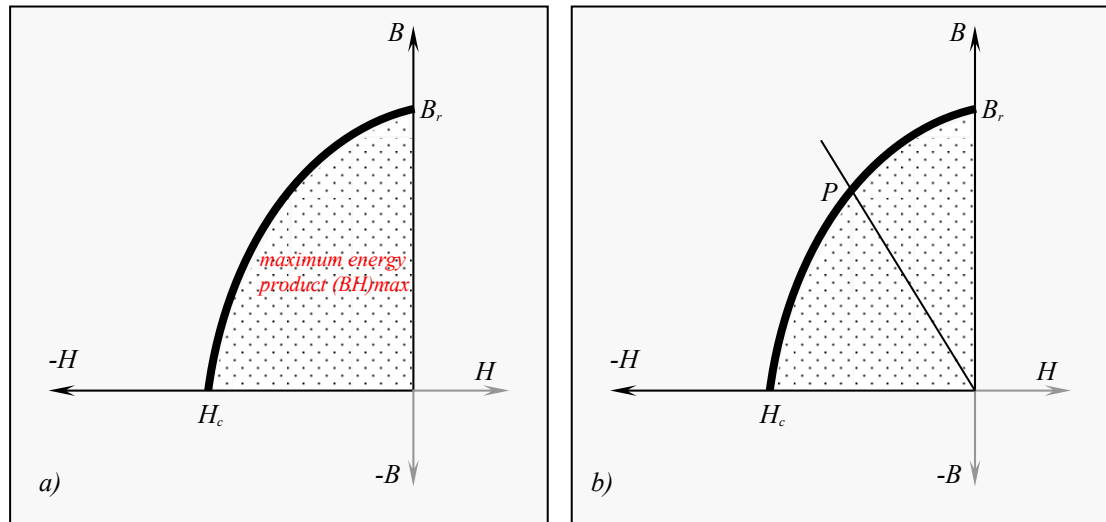


Figure 2.13. Second quadrant of the hysteresis loop: demagnetization curve (a).
Operating point P of a permanent magnet (b)

Materials that are considered hard magnetic materials are grouped in three categories: (a) permanent magnet alloys, (b) compound magnets, and (c) rare earth compound magnets. Most commonly rare earth compound used nowadays in pipeline MFL inspection tools is neodymium-iron-boron alloy, which has a very large uniaxial anisotropy, high coercivity and high-

energy product. Its high coercivity is obtained because it is difficult to nucleate reverse domains. Once a strong field magnetizes the material, the intrinsic coercivity (H_c) increases with an increase of the maximum magnetization field (H_M). This phenomenon is considered to be due to the elimination of 'magnetic seeds' for the nucleation of reverse domains by the application of H_M (Chikazumi, 1997). The maximum energy product $(BH)_{\max}$ of neodymium-iron-boron magnets can easily reach 30 megagauss-oersted (MGOe) and even goes up to 50 MGOe. Varying the number of magnets inside the tool usually changes the strength of the magnetic system in the pipeline MFL inspection tool.

Chapter 3

MAGNETIC FLUX LEAKAGE TECHNIQUE IN PIPELINE 'PIGGING' INSPECTION

3.1 Introduction

Magnetic Flux Leakage (MFL) techniques are based on magnetizing a specific test section of a ferromagnetic material and mapping its surface with some type of flux-sensitive sensor for leakage fields. Because the technique generally needs no mechanical contact with the part being evaluated and is agreeable to automatic signal recognition schemes, MFL techniques have advantages for automated, high-speed inspection. The performance of this method depends on some variables including flow velocity, variations in the material, and operating pressure.

The basic requirements of transportation oil and gas pipeline are safety and high efficiency. However 50% of the world pipe network has been used for several decades. The pipeline may occur leakage and result in danger because of erosion, abrasion, unexpected damage and so on. On the basis of plenty of studying correlative technology, it has being studied and developed high precision pipelines magnetic flux leakage on-line detection system. Magnetic flux leakage pipeline installation, for short MFL-PIG, is presently the most advanced implement of oil and gas pipeline damage in the international detection. MFL-PIG is a kind of on-line detecting robot of high and novel technology, and is also a kind of intellectual pipeline detector based on MFL non-detective test principle. The results detected by MFL method (assume excellent) are quantificational, objective and recordable (Yang, et. al., 2001).

This section considers basics necessary for an understanding of Magnetic Flux Leakage techniques applied in pipeline inspection operations. However it relates to previous section on the magnetic theory concepts.

3.2 Classification of Magnetic Inspection Techniques

A magnetic field testing technique is a method in which the magnetic field involved is static or oscillates at low frequency; otherwise (high-frequency) the method is not so classified such as microwave radiation, nuclear magnetic resonance, and electron paramagnetic resonance. In magnetic methods either currents of low frequency or currents of high frequency are used. For example, eddy current methods (high-frequency currents) are treated as magnetic field method due to their associated techniques of measurement and scanning magnetic fields. Another well-known magnetic field method is the 'magnetic particle method, which indirectly show the condition of the field from the distribution of magnetic particles on the surface of the tested material.

The magnetic-field-based nondestructive evaluation method widely described in this section is the magnetic flux leakage technique. This method exploits electromagnetic

phenomena in assessing the state or condition of the material (part) being tested. The method directly measures the magnetic phenomena being exploited (Bray and Mc Bride, 1992).

3.3 Magnetic Parameters in Magnetic Inspection Techniques

Commonly the pipeline materials, basically low-carbon steels covered by the manufacturing line pipe standard (API Spec. 5L), are ferromagnetic alloys. The parameters of saturation (B_s or M_s), remanence (B_r or M_r) and coercivity (H_c) of these steels depend of the particular chemical composition, heat and rolling treatment, residual stresses, and density of inclusions.

A rule of thumb points that approximately three times the value of the steel coercivity (H_c) is needed to magnetize common low carbon steels for the purpose of magnetic testing. However, detailed researches can find values outside typical value ranges. These typical values for industrial steel are: $B_s = 1.4-1.8$ Tesla, $H_c = 3.5 - 20$ Oe, and $B_r = 0.3-1.5$ Tesla (Bray and Stanley, 1997).

3.4 Magnetic Flux Leakage

Magnetic flux leakage (MFL) technique is accomplished on an outside artificial strong magnetic field generated by magnet; the any anomaly is detected by sensor. In other words, the magnetizing system of the MFL tool creates a magnetic field in the pipeline steel near the saturation flux density that interacts with anomalies to produce local changes (leakage) in this applied field close to the pipe's surface (Fig. 1). Although this change in magnetic properties reduces the local ability of the pipe steel to carry magnetic flux, the presence of an anomaly does not guarantee that flux will leak. As an example of this phenomenon, corrosion process changes the ferromagnetic pipe steel into non-ferromagnetic iron oxide with a evident change in the applied magnetic field, but the reduction in material alone may not cause flux leakage because the remaining material can still be able to carry the complete magnetic flux. In consequence, the interpretation of MFL signals is an important constituent in this in-line inspection technique.

The principle of magnetizing basically requires that the magnetic field should be uniform, consistent and strong enough to cause a measurable amount of magnetic flux to seep out from the pipe at local anomalies. The uniformity of the magnetic field through the pipe wall and its consistence along the pipeline length is needed to produce accurate linear signals and to make possible adequate comparisons among different local measurement, respectively.

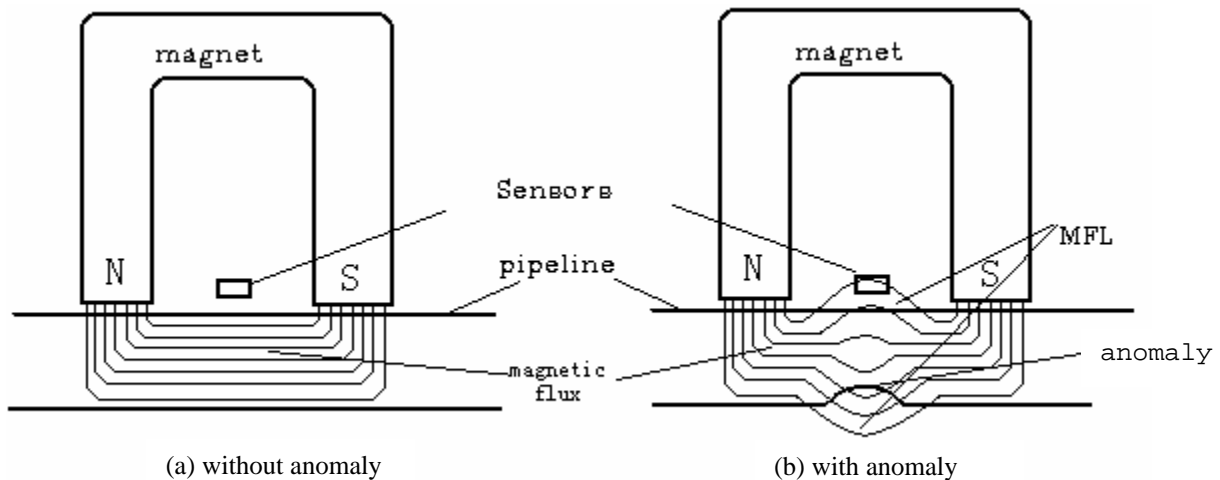


Figure 1. Magnetic field in the pipeline steel created by a Magnetic Flux Leakage tool (without anomaly, a) and local changes or leakage in this applied field close to the pipe's surface due to an anomaly (with anomaly, b) (Yang *et al*, 2001).

Most two important variables that impact magnetization are the applied magnetic field intensity (H) and the flux density (B , or magnetization M) in the pipe material. The relationship between both variables is nonlinear in ferromagnetic materials, as it is explained in previous sections. There will be a relatively smaller magnetic flux increase at the higher magnetic field intensity than for the same change in flux at lower field intensities. The ratio flux density/magnetic field intensity of the steel magnetization curve is known as the magnetic permeability of the alloy. Ferromagnetic materials such as low-alloy-carbon steels, which are normally attracted by a magnetic field, have an extraordinary permeability. However, the permeability of ferromagnetic materials changes with the magnetic field intensity and can only be considered constant for relative small change in it. Additionally, a narrowing in the pipe wall thickness causes a reduction of the magnetic permeability of the material producing the flux to leakage in alternative direction.

On the other hand, Nestleroth and Bubenik related permeability to flux density saturation, which is defined as the magnetization degree beyond which an increase provides no significant change in magnetic flux density (Fig. 2). Nevertheless, some other authors relate saturation to normal magnetization curve. They called saturation to the effect where the flux density levels off with increasing amounts of magnetic field intensity.

MFL tools are usually designed to create different magnetization levels. In corrosion based metal-loss systems magnetic saturation is applied in the pipe wall thickness in which a narrowing in material will cause flux leakage. While in mechanical damage systems, MFL tool is designed to produce lower magnetic intensity degrees. In addition, pipe wall thickness is another issue to be considered during MFL tool design. Nestleroth and Bubenik (1999) point that variations in wall thickness will change the

applied magnetic field intensity, i.e. heavier wall thickness stronger magnetic field intensity needed (Fig. 3).

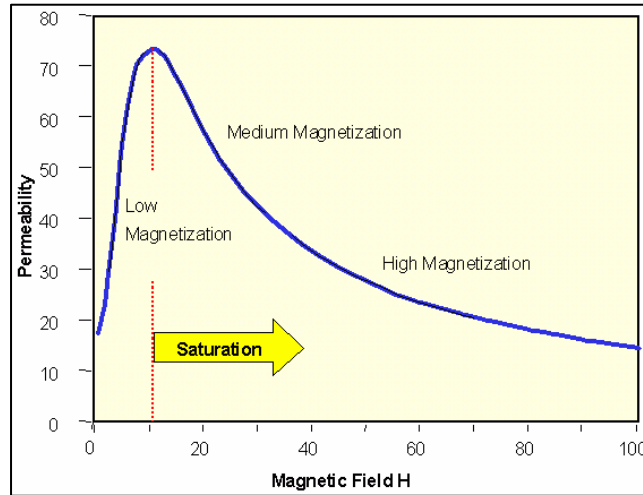


Figure 2. Applied magnetic field intensity and permeability curve of a specific material (Nestleroth and Bubenik, 1999).

The induced magnetic field intensity is affected by other parameters, as well, such as variation of material properties, characteristics of magnet-pipe wall contact, MFL tool velocity, and remnant magnetization. The remnant magnetization is the most influential factor as proposed in this work.

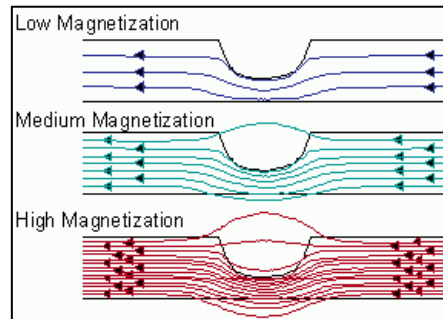


Figure 3. Pipeline wall thickness effect on applied magnetic field intensity (Nestleroth and Bubenik, 1999).

From physics standpoint, when low-carbon steel is magnetized in one direction, it will not relax back to zero magnetization when the imposed magnetizing field is removed. The amount of magnetization it retains at zero driving fields is called its remnant magnetization or ‘remanence’. If an alternating magnetic field is applied to the

material, its magnetization will trace out a loop called a ‘hysteresis’. Since it was explained, the lack of retrace ability of the magnetization or hysteresis is related to the existence of magnetic domains in the material. Once the magnetic domains are reoriented, it takes some energy to turn them back again (Nave, 2002).

From pipeline inspection standpoint, the remnant magnetization is the magnetic flux density degree left in the pipe material after a MFL tool goes by. The remnant magnetization significantly influences the detection and characterization of metal-loss regions. Based on the principle of hysteresis, when the induced magnetic field is removed a magnetization level is locally left in the pipe. Once the pipe steel is re-magnetized, the magnetization curve begins at applied magnetic field intensity equal to zero and a magnetic flux density equal to the remnant flux density.

Figure 5 schematically explains the basics of this phenomenon in pigging operations. Because remnant magnetization changes the applied flux levels, it also affects the flux leakage field and the ability to detect and characterize metal loss. The effect of remnant magnetization is a function of defect geometry and number of repeated magnetizations. The remnant magnetization effects reach a limit after 3-5 magnetizations, where flux leakage fields significantly drop (Nestleroth and Bubenik, 1999).

3.5 Inspection of Pipeline Using MFL Techniques

Although MFL technique does not discriminate between types of anomalies (cracks, metal-loss defects and inclusions) and is the most common in-line inspection technique used in pipeline evaluation testing, its significant limitation is that it is only applied to ferromagnetic and magnetically permeable alloys. Many relevant characteristics make MFL technique a useful method of inspection.

The MFL tool sensitivity is limited only by environment noise and magnetic field strength. However, high-sensitivity MFL tools have been developed to detect small-scale surface and near-surface anomalies in pipeline materials.

High-Sensitivity MFL Techniques

Very small material anomalies are usually detected by magnetic techniques that work at magnetic field strength level below the saturation value. A very high signal/noise ratio is possible to obtain when the noise level is almost negligible, and it can be achieved when the alloy is magnetized below the knee of the hysteresis curve (half length of a-b curve, Fig. 2.7, Chapter 2). It means, when performing inspection in active field (explain in further section).

A limitation of the high-sensitivity methods is that they are not very useful in discriminating surface cracks and near-surface inclusions. These techniques, a simple extension of the MFL technique, were known as magnetic field perturbation method.

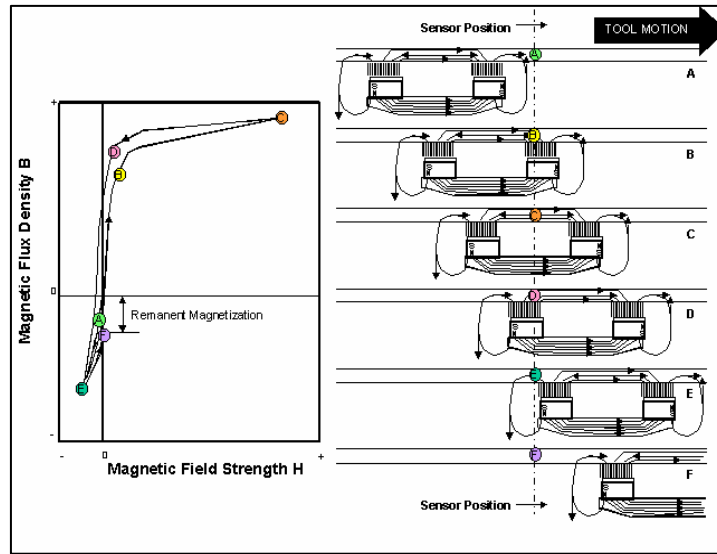


Figure 5. Basics of remnant magnetization phenomenon in pigging operations (Nestleroth and Bubenik, 1999).

3.6 Field Levels in Magnetic Flux Leakage

Although no universal rules regarding field levels for MFL inspection it is well known that magnetic flux leakage depends strongly on the applied magnetization level. The magnetization process should be capable to produce a high flux leakage in order to detect the smallest defect in the pipeline section. In other words, at low active magnetic field the material close to anomaly is not highly magnetized, while at high active field the material in the vicinity of the slot is higher, and the high density of flux lines is equivalent to the theoretical optimum magnetization level (section 3.4). When the density of the flux lines is high (or at high residual induction) most of the material is close to the remanence magnetization or B_r , and the material close to the anomaly cannot have an induction that is greater than B_r , therefore the additional flux is forced out.

The field intensity in the pipeline material must be raised to such a level that there is an adequate MFL from the defects. At low levels, as in Fig. 3 (low magnetization level), the diversion of flux merely raises the material around the discontinuity to a higher level of induction; it means, no resulting magnetic flux leakage. At higher applied levels, as the permeability ($\mu = B/H$) falls, the relative reluctance of the material around the flaw rises in comparison to that of the flaw, and eventually, magnetic flux leakage is produced (Fig. 3, high magnetization). There may be little detectable MFL is the material is not close to saturation. In this situation the depth of a subsurface anomaly causes the surface MFL pattern to broaden, and its width is similar to that of surface noise caused by local permeability variations. Nevertheless, in common pipeline inspection operations, the alloy is saturated and noise-reduction sensors and electronics are used (Bray and Stanley, 1997).

Since irregularities and small differences in permeability are dominant causes of surface geometrical eccentricity of circumferentially magnetized tubes represents a common motive of surface noise in pipeline inspection. Nestleroth and Bubenik, (1999) state that variations in wall thickness will change the applied field intensity, especially when the tool is designed to operate at medium magnetization levels. Typical wall thickness variations in welded pipe are small, but variations in seamless pipe can range from 5 to 20 percent. These variations increase or decrease the applied flux density. By considering conservation of flux, the flux in two different points (a and b) in the cross-section of a eccentric pipe, and the flux density at the external surface (B_R) (Fig. 8), the total leakage flux is

$$\Phi_{\text{leakage}} = (A_A - A_C) B_R \quad (3.6)$$

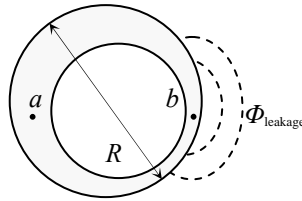


Figure 8. Eccentric circumferentially magnetized tube.

CHAPTER 4

EFFECTS OF HYDROGEN IN PIPELINE STEELS

4.1 Introduction

Hydrogen may comprise the most studied element in the application of metallurgical phenomena in the oil and gas industry because its ubiquitous presence in solution in iron and steel. Hydrogen is a problem in steel because it is highly mobile as an atom and can both diffuse through the lattice and be transported by the movement of dislocations. In the present chapter attention is focused on the influence of hydrogen on the pipeline steels properties and performance.

Even the limited area of hydrogen in iron and steel, the literature is so large that only a restricted number of references can be included in the discussion. Reviews of the subject from several viewpoints have attended, including hydrogen solubility, diffusion, permeation, removal, and sources, as well as the phenomenology of hydrogen damage in steel and weldments, the hydrogen measurement, and the hydrogen influence on magnetic behavior of iron and steel.

4.2 Solubility

The concentration of a diatomic gas such as hydrogen (H_2 , one of the two lightest nuclear isotopes) in metals is proportional to the square root of its observed pressure (Sievert's law), as following

$$C_H = k (P_{H_2})^{1/2} \quad (4.1)$$

where k is a constant. Sievert's law, based on the thermal equilibrium reaction of atomic and molecular hydrogen, defines k as $\alpha e^{(-\Delta H/RT)}$, where ΔH is the enthalpy change. However, Hirth (1980), based on a compendium of experimental data, prefers to use k as $0.00185 e^{(-3440/T)}$, where T is in $^{\circ}K$.

This effect of pressure makes the solubility (S) of hydrogen in iron a pressure-dependent function; however, two more parameters affect it: crystal structure (basically, FCC or BCC) and temperature.

From the iron-hydrogen system equilibrium diagram (Fig. 1), it is well known that the solubility of hydrogen in liquid iron is higher than the solubility in any solid phase of iron because the liquid phase is fully relaxed and there is no lattice distortion to impose a condition on the occupation of the interstitial sites (Pepperhoff and Acet, 2001). The solid solubility in FCC γ -iron is higher than in BCC α -iron. Increase the temperature of the system makes greater both iron solubilities.

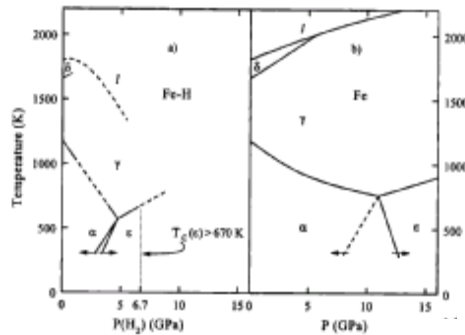


Fig. 1. Pressure-Temperature diagram of iron and iron-hydrogen system (Pepperhoff and Acet, 2001).

Other characteristic features can be summarized as follow: (1) Hydrogen promotes the stabilization of the densely packed ϵ and γ phases, i.e. the lattice is transformed into close-packed structures at reasonably low hydrogen pressure. (2) The closed-packed structure appears in the order hcp-dhcp-fcc with increasing temperature (Fukai *et al*, 2000). (3) The triple point α - γ - ϵ is reached at low pressure and temperature. (4) The Fe melting temperature or melting point is drastically reduced in Fe-H system (characteristic feature of interstitial alloys). (5) In the solid state, the interstitial atoms cause lattice distortions that prevent all possible interstitial sites to be occupied. (6) At pressures above 10 GPa the ϵ -Fe-H phase melts already at very low temperatures (Pepperhoff and Acet, 2001).

At temperature above 400°C dissolved hydrogen is contained as atomic hydrogen in the interstices of the metal lattice. On the other hand, at lower temperatures a excess of hydrogen is observed (interstitially insoluble), which is retained in other sides in the steel commonly referred to as “traps”. Interrante (1982) state that the hydrogen content, the apparent or measured solubility, can be greater than the solubility limit of the lattice and the excess amount of hydrogen is trapped in various sites that apparently do not affect solubility at high temperature. Further, at room temperature, the dissolved hydrogen may be only a small fraction of the total hydrogen content.

The apparent solubility of steel is considerably increased by factors such as the presence of nonmetallic inclusions and cold working because they tend to increase the number of trapping sites or the volume of internal voids. In other words, the saturation concentration of hydrogen in steel increases as much as the amount of cold work does. Other external factors that affect the effective pressure hydrogen in the system can significantly act on the saturation concentration and the rate of absorption of hydrogen into the steel. One of these factors is the pH of a aqueous charging medium. Some authors reveal that the saturation concentration rises from about 1 ppm at pH of close to 8 to approximately 30 ppm at a pH of 1.4. It is because the effective pressure of hydrogen at acid range is greater than that at pH above 8.

4.3 Diffusivity

Diffusion is a kinetic process that leads to the homogenization, or uniform mixing, of the chemical components in a phase. Diffusive mixing in solids occurs on the atomic or molecular level. As time increases, the extent of homogenization by diffusion also increases, and the length scale over which chemical homogeneity persists within a phase gradually extends to macroscopic distances. Diffusion that results in the net transport of matter over such macroscopic distances is considered to be a non-equilibrium process, insofar as it ceases when the phase eventually achieves full thermodynamic equilibrium (Glicksman, 2000).

Since the hydrogen molecules are relatively large and only the smaller atomic form of hydrogen can diffuse effectively through the steel lattice, the migration of atoms from one part to another of the lattice represents the mainly cause of the movement of hydrogen inside the steel.

The hydrogen atom dissociates into a proton and an electron ($H^0 \Leftrightarrow H^+ + e^-$) in the metal. The protons occupy interstitial positions and the electrons are introduced into the d-band of the metal. Compared to the size of the interstitial sites, the protons are vanishingly small. However, the positive charge of the protons has to be screened in order to preserve electrical neutrality. The screening occurs by the formation of an electronic cloud of atomic dimensions (the covalent radius of the hydrogen atom is 0.053 nm). However, the screening is not perfect, and repulsive forces occur between the proton and the neighboring positively charged metal nuclei. This leads to a local expansion and thereby a distortion of the lattice. Therefore dissolved hydrogen in metals implies a proton with a screening electron cloud (Pepperhoff and Acet, 2001).

The driving force for the diffusion of hydrogen is a gradient in the chemical potential which results either from a gradient in the lattice hydrogen concentration or from a gradient in the hydrostatic component of an elastic stress field (Interrante, 1982). It means, the hydrogen migrates from a region of high chemical potential (e.g. higher interstitial concentration) to a region of low chemical potential until the equilibrium is achieved. In addition to the motivation of a gradient in the chemical potential, both a gradient in an electric field and a gradient in temperature may motivate the diffusion of hydrogen in steel. Therefore, the degree of diffusion is affected by the hydrogen concentration and the lattice diffusivity (D).

Driving forces for diffusion can be afforded by stress gradient factors such as notches, cracks, inclusions, and bending moments, as well as by the elastic stress field of a dislocation. These elastic stress fields (regions of biaxiality), to which the hydrogen diffuses, in this instance, are tensile in character. In the regions of biaxiality, the energy of the interstitial hydrogen is higher than that in the regions of triaxiality, which are known as regions of locally increased solubility because hydrogen atoms diffuse preferentially into these regions. It means the bigger triaxial component, the greater the amount of hydrogen that diffuses. Once external stresses are released regions of

triaxiality reduce absorption of hydrogen and local super-saturation can be achieved. Therefore, precipitation of hydrogen from the solution in the lattice is possible as well as chemical reaction.

The lattice diffusivity can be related to the hydrogen pressure and temperature (T , absolute temperature) by the Arrhenius equation

$$D = D_0 e^{-Q_g/RT} \quad (4.2)$$

where D_0 is a pre-exponential term (including the effect of hydrogen pressure), Q is the activation energy, and R the universal gas constant. Since hydrogen solubility is lowest in the BCC α -iron (see Fig.), and it is noticeably higher in the FCC γ -iron and, yet, higher in the DHCP ϵ -iron, the lattice diffusivity of hydrogen in latter phases (ϵ and γ) is much lower than in α -phase. Lattice diffusivity is still lower in austenitic stainless steel because of the relatively high alloy content.

Glicksman (2000) points that hydrogen diffusion in metals occurs under a wide variety of environmental interactions: aqueous corrosion, electrolysis, electroplating, and welding. In many of these processes and applications cold-worked metals are used due to they high dislocation density.

4.4 Trapping

The energy of motion (G_m) of the hydrogen atom and the features of the traps control both the jump probability of the hydrogen atoms and the tendency of hydrogen to be trapped. Microstructure consisting of a uniform distribution of fine and strong hydrogen traps may increase an alloy-hydrogen attack resistance. The relationship of the energy of motion and the positions of the hydrogen atom moving through a series of equilibrium positions in a lattice is represented by the sinusoidal line in Fig.2-4, where the E_d (proportional to the activation energy, Q) is the amplitude of this wavy line.

Pressouyre (1979) states that when a hydrogen atom jumps from a normal lattice site into a trap (where hydrogen will be accumulate internally as trapped H_2 molecules), the probability of an eventual return to the former site is decreased. There are two main reasons why, in a crystal lattice, jump probabilities should be modified. There are driving forces (for diffusion) that push the hydrogen atom into a preferential direction, make it more facile, and thus more probable, for the atom in the point B to jump (forward) to point A than to jump (backward) to point C (Fig. 2a), therefore the atom is preferentially attracted to site A. In that case, the lattice is not modified. However, the lattice may be completely modified (Fig. 2b), i.e. the average jump height is changing from site to site, and the frequency is affected. In this case the forward jump is made easier by the lattice being stretched open (tension).

The energy of the trap E_T and the features of the trap governed the tendency of the trap to hold hydrogen atoms. There two extreme types of traps: attractive traps (Fig. 2c), a region of the lattice where the hydrogen atoms are subjected to attractive forces (electrical fields, stress fields, temperature gradients, and chemical potential gradient), and physical traps (Fig. 2d), a modification of the ideal crystal lattice where energetic conditions make it more favorable for hydrogen to keep on. Because of it is less difficult for a hydrogen atom to jump out from a attractive trap than from a physical one for the same energy value E_T , an attractive trap is considered an reversible trap where hydrogen atom can easily both come in or leave. In conclusion, the amount of hydrogen atoms trapped at any confined site depends of the driving forces, the local concentration of hydrogen, and the characteristics of the traps. The traps in which the hydrogen atoms are trapped can build up without restraint (i.e., large hydrogen concentration) and are called unsaturable traps (Fig. 3).

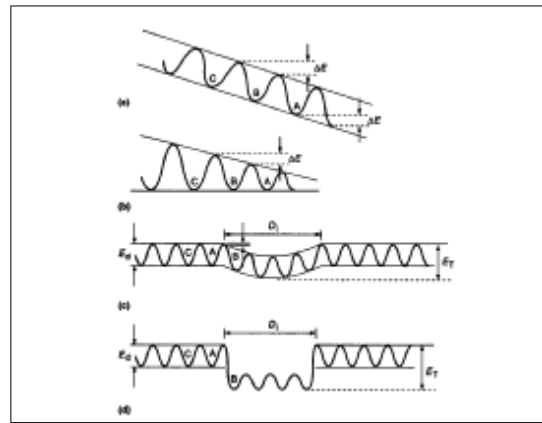
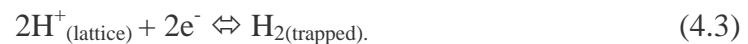


Fig. 2. Schematic of energy steps necessary to the diffusion of hydrogen atoms through a metal lattice (Interrante, 1982).

In metals containing large concentration of lattice hydrogen, the trapped H_2 pressures can approach enormous values. The equilibrium between the trapped molecular hydrogen in a unsaturable trap and the lattice's atomic hydrogen is governed by the common dissociation reaction



The valence band of the metal (to which electrons from molecular hydrogen dissociation go) cedes the required electrons to balance the ionization in the trapping reaction (Eq. above) and neutralize the interstitial protons. Iron and its alloys are capable of dissolving high concentration of lattice hydrogen showing a high density of electronic states in their d -bands. Glicksman (2000) points that the concentration of molecular hydrogen in traps, and the concentration of H^+ in interstitial sites, may be related through

the well-known mass-action principle applied to the dissociation reaction. The law of mass-action states,

$$K(T) = [H^+]^2 / [H_2] \quad (4.4)$$

where $[H_2]$ represents the concentration of trapped molecular hydrogen, C_{H_2} , $[H^+]$ is the concentration of protons, C_{H^+} , dissolved interstitially in the lattice, and $K(T)$ is the equilibrium constant. Therefore, the equilibrium constant for the dissociation reaction may be expressed as the concentration ratio of dissolved lattice hydrogen to molecular hydrogen,

$$K(T) = (C_{H^+})^2 / C_{H_2}. \quad (4.5)$$

Insofar as the hydrogen within the metal resides in two distinct forms (trapped molecular H_2 and untrapped H^+) Fick's second law for the overall diffusion of hydrogen in the material must be modified. Specifically, the Fick's second law relates the time variation of the total hydrogen concentration (trapped H_2 plus the untrapped protons) with the divergence of the flux of mobile hydrogen (H^+ only). The relationship at low temperature of the experimentally observed diffusivity, D_{eff} , and the lattice diffusivity, D_{H^+} , is given by

$$D_{\text{eff}} = D_{H^+} C_{H^+} / 2 C_{H_2}. \quad (4.6)$$

Johnson and Lin (1980) affirm that there is another important class of potential trapping sites called *saturable traps*. Plausible physical arguments suggest that the capacity for hydrogen of these traps (dislocations, impurity atoms, and internal interfaces) is finite. In this model the trapped hydrogen concentration then saturates as the lattice hydrogen concentration is increased. The saturation concentration is equal to the trap density. In this case the diffusion kinetics, especially at low temperature and low lattice concentration, is governed by the trapped concentration.

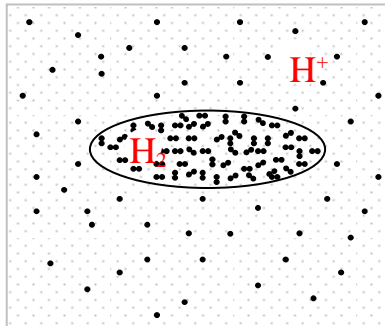


Fig. 3. Trapped H_2 molecules in a trap surrounded by a lattice saturated with interstitial H^+ .

In conclusion, Pressouyre (1979) classifies hydrogen traps in steels according to size: point (element such as Mn, Cr, Ti, Nb, etc.), linear (dislocations), planar or bidimensional (particle interfaces, grain boundaries, etc.), and volume (voids, cracks, and particles). This classification is still currently applied. Jones (1996) states that these traps may be reversible or irreversible, depending on whether the trapped hydrogen is easily release (time necessary to reach some critical local hydrogen concentration) or tightly bound, as measured by the interaction energy listed in Pressouyre classification. In addition, the traps may be mobile (dislocations) or stationary (solute atoms, particles, grain boundaries).

4.5 Hydrogen Permeation

The diffusant, in many steady-state diffusion processes, is the gas that is forced into the free surface of the material by application of different partial pressures, which result in different equilibrium concentrations inside the solid. The local solid-gas interface equilibrium conditions (equal thermodynamic activities) control the steady-state solubility of the diffusant in the surface. In the solid-gas interface the dissociation reaction of gas molecules take place in order to form single species that can more easily enter the solid. Since the hydrogen gaseous diffusion (permeation) into the solid is preceded by the dissociation reaction



the mass-action law is considered to determine the equilibrium constant of this reaction:

$$K(T) = [\text{H}] / [\text{H}_2]^{1/2}, \quad (4.8)$$

which is equivalent to the Sievert's law (Glicksman, 2000):

$$K(T) = S / P_{\text{H}_2}^{1/2}. \quad (4.9)$$

The concentration gradient responsible for hydrogen diffusion can be defined in terms of the concentration differences (input surface concentration – output surface concentration). The permeation rate, P , at which the hydrogen passes through a wall or membrane of the steel of fixed thickness, L , is established by the diffusivity and the concentration gradient as

$$P = D (C_1 - C_2) / L. \quad (4.10)$$

The values of C_1 and C_2 are known as the interstitial solubilities at the input and output surfaces, when these areas are at equilibrium with their corresponding environments. In terms of Sievert's law, the permeation equation becomes

$$P = D (S_2 - S_1) / L. \quad (4.11)$$

Trapping either at higher temperatures or at lower temperatures does not inhibit the diffusion after the steady-state condition of permeation has been obtained and traps are filled to the level appropriate for the hydrogen concentration that exists through the steel. Before the traps are filled at lower temperatures, the determination of the permeation of hydrogen is possible by the permeation equation ($P = D (C_1 - C_2)/L$); however, afterward trapping will occur and hinder the diffusion, in consequence measured values of C_1 and C_2 will not represent the equilibrium concentration, which govern the steady-state rate (P_∞). When they are completely filled, steady state permeation occurs at a rate controlled by the interstitial concentration gradient. Thus the results measurements of steady-state permeabilities will be indicative of the interstitial diffusion rate, but while the traps are being filled, the permeation behavior will also be influenced by the trapping behavior (Interrante, 1982).

4.7 Sources of Hydrogen

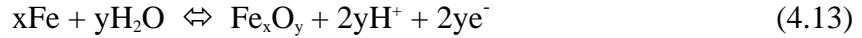
Dissolving hydrogen in iron is an endothermic process and therefore requires energy. The main reason for the low solubility is the very low atomic hydrogen concentration in hydrogen gas under normal conditions. To investigate the influence of hydrogen on the physical properties of iron requires, however, larger quantities that can only be introduced if the surface of iron can be supplied with atomic hydrogen in larger quantities. This can be achieved by the cathodic charging of iron with electrolytically produced hydrogen in the nascent state (Pepperhoff and Acet, 2001).

From oil and gas pipeline design standpoint, hydrogen may be made available to metal surface from various sources such as hydrogen-gearing environments during welding, heat-treatment, pickling or service. The most common sources are the cathodic reduction of hydrogen and water, which can be present during cathodic protection or corrosion:

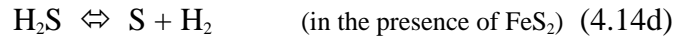
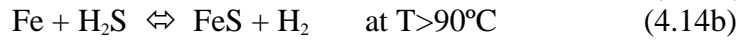
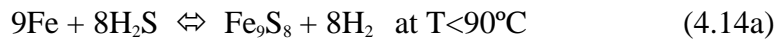


Processes involving cathodic polarization, such as cathodic protection and electroplating, accelerate hydrogen formation by the cathodic reduction equations (Jones, 1996). The electrons required to make possible these reactions are supplied either by impressed current rectifiers or by sacrificial anodes.

On the other hand, when steel come in contact with aqueous environment another source of hydrogen takes place, the atomic hydrogen liberation from the iron-water reaction:



In addition, when steel pipeline carries H₂S-containing hydrocarbon fluids two new potential hydrogen sources may be present, the diatomic hydrogen liberation from the iron-H₂S reactions and from the dissociation of hydrogen sulfide (Craig, 1993):



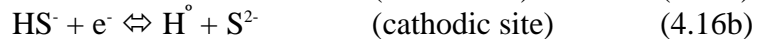
However, some authors refer the general corrosion reaction $\text{H}_2\text{S} + \text{Fe} \Leftrightarrow \text{FeS} + 2\text{H}$ to describe the interaction of steel and the H₂S-containing environment. Furthermore, in sour environment when it comes in contact with water the H₂S can dissociates in ions according to (Serna *et al*, 2003):



and



Then a corrosion reaction occurs with steel thus forming ferrous ion at anodic sites and reduction of hydrogen at cathodic sites at the steel surface, according to:



It has found that the high strength pipeline steel grades are susceptible to hydrogen embrittlement (HE) and most of the HE failures have been related to the sulfide stress cracking (SSC) susceptibility. SSC is one of the major failure problems that occur in oil and gas pipeline steel when they are exposed to aqueous H₂S environments.

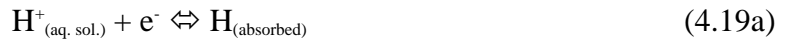
Another important source of hydrogen can take place when CO₂, one of three primary corrodents (CO₂, H₂S, and O₂) in oil and gas production, dissolves in water and corrosion of steel occurs. The reaction that most often predominates is (Craig, 2002):



Additionally, Craig (2002) affirms that when water produced from oil and gas wells are handled at the surface (wellhead equipments and pipelines), it may eventually be in contact with air. Many basic forms of corrosion products may appear with dissolved oxygen in the water. However, hydrogen may be made available from two reactions that occur only for the gamma form of iron oxide (FeO):



Once the atomic hydrogen H⁺ is on the cathodic steel surface, the electrons provided by cathodic protection equipments assists to produce absorbed hydrogen, which can be either absorbed by the steel or recombined to form molecular hydrogen:



The degree of absorption of hydrogen and the recombination reactions are hardly affected by the action of surface absorbents called “poisons” and inhibitors. The hydrogen entry is enhanced by dissolved “poisons” (or cathodic poisons), which are commonly ions that retard the formation of molecular hydrogen and increase the resident time of nascent hydrogen on the surface. The well known poisons include phosphorous, arsenic, antimony, sulfur, selenium, tellurium, cyanide, and their compounds (Jones, 1996). In the presence of sulfide, the hydrogen recombination reaction is retarded so that the hydrogen atoms diffuse into the steel rather than recombining on the steel surface (Lee *et al*, 2003). The inhibitors are usually polar organic compounds that commonly block either the absorption of absorbed hydrogen or the anodic reaction by forming chemisorptive bonds on active surface sites (Interrante, 1982).

Some studies have revealed that hydrogen damage in iron and steels is significantly more aggressive in environment containing H₂S than in gaseous H₂. The explanation of this phenomenon is based on the velocity of absorption kinetics. Although at low temperature (80°F ~ 26°C) and on essentially pure iron surfaces, the difference is fundamentally neglected, on steel surfaces alloying elements and impurities enhance hydrogen absorption from H₂S environments. It is considerably important regarding to pipeline steels for oil and gas transport.

4.8 Environmentally Induced Cracking – Hydrogen Damage

Environmentally induced cracking include four forms of corrosion that produce cracking of metallic materials exposure to particular environments. These phenomena are hydrogen damage (usually also known as hydrogen embrittlement), stress corrosion cracking, liquid-metal embrittlement, and solid-metal induced embrittlement. Generally, these forms of environmentally assisted cracking exhibit some similarities such as their common dependence on yield strength and applied stress. Even though there are various theories that are specific to the behavior of certain materials or environments, none for any of those mechanisms totally explains all behavior observed either under laboratory or field conditions.

As propose of this work, hydrogen damage (or hydrogen embrittlement, improper term used to describe a multitude of failure modes involving hydrogen) will be considered as the most relevant environmentally induced cracking phenomenon. ASM Handbook Vol. 13A (2003) classifies hydrogen damage phenomenon, a form of environmentally induced cracking that generally occurs as a result of the combined action of hydrogen and applied or residual tensile stress, into different types of processes of hydrogen degradation of metals:

4.8.1 Hydrogen Embrittlement.

Hydrogen environment embrittlement occurs during the plastic deformation of alloys in contact with hydrogen-bearing gases or a corrosive reaction and is therefore strain rate dependent. The degradation of the mechanical properties of the material depends on the strain rate and the hydrogen pressure and purity.

Hydrogen stress cracking (commonly known as hydrogen-induced cracking or static fatigue) is characterized by the brittle fracture of a typically ductile alloy under continued load in the existence of hydrogen. Generally, fracture takes place at sustained loads lower than the yield strength of the alloy. This cracking mechanism, commonly considered a sub-critical crack growth mechanism that often produces time-delayed fractures, depends on the hydrogen fugacity, strength level of the material, heat treatment/microstructure, applied stress, and temperature.

Hydrogen stress cracking, which promotes one mode of fracture and produces sharp singular cracks, is associated with the absorption of hydrogen and a delayed time to failure (called incubation time) during which hydrogen diffuse into regions of high triaxial stress. The catastrophic cracking of steels in H₂S environments (common environment in oil and gas pipelines services), referred to as sulfide stress cracking-SSC, is a special case of hydrogen stress cracking.

Zhao, *et al* (2003) points that sulfide stress cracking is the main failure mechanism of hydrogen embrittlement for high-strength pipeline steels, and that pipeline steels are susceptible to SSC in aqueous H₂S environment with the imposed stress, even if their strength values have been limited to the critical yield strength for sour service (Hardness Rockwell C 22 or 690 MPa).

Jones (1996) defines H₂S as one of the most aggressive of the common industrial aqueous corrosive solutes. The sulfide anion acts as a poison that retards recombination of nascent H-atoms on corroding surfaces, increasing the residence time of nascent H, and enhances hydrogen penetration into the metal lattice.

Loss in tensile ductility, one of the earliest distinguished types of hydrogen damage, generally occurs in lower-strength alloys that experience decrease in elongation and reduction in area. The loss in tensile ductility is a function of hydrogen content of the material and strain rate.

4.8.2 Blistering, Hydrogen Attack, Metal Hydride Formation, Shatter Cracks, Flakes, Fisheyes, Microperforations, and Degradation in Flow Properties

Blistering occurs primarily in low-strength alloys when sufficient hydrogen builds up at crystalline or metallurgical inhomogeneities (traps) and then atomic or nascent hydrogen precipitates as molecular hydrogen (H₂). The pressure developed by molecular hydrogen can achieve sufficient high values to rupture interatomic bonds, forming microscopic voids and macroscopic blisters (Jones, 1996). Blisters are frequently found in low-strength steels that have been exposed to aggressive corrosive environment (such as H₂S) or cleaned by pickling (ASM Handbook Vol. 13A, 2003).

Hydrogen attack is a elevated-temperature phenomenon, in which hydrogen reacts with metal substrates or alloys additions such as carbides and carbon to form decarburized structures and methane gas. Thus, this form of hydrogen damage occurs in carbon and low-alloy steels exposed for long time to elevated-pressure hydrogen at high temperature (above 200°C or 400°F).

Metal hydride formation produces embrittlement in some metals and their alloys due to the precipitation of metal hydride phases. Above 250°C, dissolved hydrogen (obtained often from welding, heat treating, during melting of the alloy, and/or corrosion process) reacts with titanium, tantalum, niobium, vanadium, uranium, magnesium, thorium, and zirconium to form brittle hydrides. The

degradation of mechanical properties of these metals and their alloys is because hydrides increase tensile strength and decrease ductility.

Shatter cracks, flakes, and fisheyes are common characteristics observed in castings, weldments, and forgings affected by hydrogen damage. Hydrogen obtained from melting process (hydrogen solubility in liquid phase is higher than it in solid phase) diffuses during the cooling process (below 200°C ~ 400°F) to and precipitates in metallurgical inhomogeneities such as voids and discontinuities. In consequence, the hydrogen solubility in the solid alloy decreases causing embrittled regions around inclusions, precipitates, and laminations by supersaturated hydrogen. It may be considered a special case of blistering due to its comparable features.

Fisheyes are sometimes evident on the brittle fracture surface of tensile specimens taken from plates or forgings of high hydrogen content. Fisheyes are often associated with microscopic pores on inclusion on the fracture surface. Baking or long-term room-temperature aging will sometime eliminates fisheyes and restore normal ductility (Jones, 1996).

Micro-perforations by elevated-pressure hydrogen occurs principally in iron and steels and are characterized by a group of diminutive holes or pits that permit infiltration of gases or fluids through the alloy surface. This phenomenon is possible because of the presence of a extremely high-pressure hydrogen environment at room-temperature.

Degradation in flow properties in hydrogen atmosphere occurs predominantly in iron and steels at room-temperature and its mechanism is based on absorption of hydrogen from either environment or internal surrounding areas to dislocations. This phenomenon occurs also in nickel-base alloys at elevated temperatures.

4.9 Hydrogen Damage Mechanism

Since hydrogen damage is a complex phenomenon, in the last fifty years various metallurgical mechanisms to explain these various forms of hydrogen degradation have been suggested. Although several authors have shown that so-called internal and external hydrogen damage are distinguished by hydrogen being present uniformly or in a gradient from the surface, they are not characterized by inherent different mechanism (Hirth, 1980). Even though some other mechanisms have been recommended, most are considered variations on these basic theories.

4.9.1 The hydrogen pressure theory assumes that embrittlement is caused by the diffusion of atomic hydrogen into the metal and its accumulation in the structure crystalline (dislocations) and metallurgical defects such as microvoids and second-phase interfaces. A high concentration of hydrogen at

these microstructural inhomogeneities causes a large internal pressure that enhances micro-void growth and crack initiation.

Since hydrogen charged into steel at high fugacity during aqueous corrosion or cathodic charging may also produce an elevated pressure at these discontinuities, hydrogen stress cracking failures can be caused by charging hydrogen into the steel either with elevated-pressure hydrogen gas or under intense electrochemical charging. On the other hand, even when the source of hydrogen was at low fugacity, dislocation transport can also create high internal pressure in micro-voids.

4.9.2 *The reduced surface energy or surface absorption theory* states that the absorption of hydrogen adjacent to crack tip decreases the surface free energy of the metal and suitably the work of fracture, which enhances crack propagation. Although there are some arguments against this theory, it may explain the crack propagation of high-strength steels in low-pressure hydrogen environment.

4.9.3 *The de-cohesion theory* describe the dissolved hydrogen effect of the bond strength (or cohesive force) between atoms of the alloy matrix. Hydrogen tends to diffuse and accumulate ahead of a crack tip (known as a region of hydrostatic tensile stress) to lower the cohesive force between metal atoms. This weakening of bond strength makes the normal maximum tensile stress perpendicular to the crack plane equal to or bigger than the lattice bond strength causing fracture.

4.9.4 *The enhanced plastic flow theory* is based on fractographic evidence from crack surfaces and has been related to hydrogen dislocations interactions. This mechanism suggests that hydrogen increases dislocation kinetics and creates new dislocations at surfaces (such as crack tip). In consequence, this hydrogen damage phenomenon induces to reducing locally the material strength and enhancing localized plasticity. ASM Handbook Vol. 13A (2003) affirms that although this behavior (softening by hydrogen) has been observed in certain steels, hardening by hydrogen has also been found.

Troiano (1984) states that a combination of hydrogen and internal stress is required for crack nucleation; for example, the enhanced dislocation motion is not itself a model but is a contributing factor to an overall degradation process. It has also been stated that the major effect of hydrogen is to promote the injection of dislocations at the surface (crack tip).

Since hydrogen is a relevant factor to cause crack nucleation, it first has to be transported through the solution (environment) to the metal surface, absorbed, and then transported internally by diffusion mechanism or dislocation kinetics. Finally, it will be accumulated at a specific internal

location (such as internal interface) where it has an effect on nucleation and growth of a crack.

4.9.5 *Hydrogen attack*, a strictly high-temperature mechanism, refers to internal (above 200°C) decarburization or surface (above 540°C) decarburization of steels, however the mechanism is predominantly the same for both forms. This behavior is defined as a phenomenon that depends on temperature, time, and hydrogen partial pressure.

4.9.6 *Hydride formation* is the degradation of transition metals and their alloys in hydrogen atmospheres by a mechanism of formation of brittle metal hydrides phase at the crack tip. When sufficient hydrogen is available in the alloy, a metal hydride precipitates. Cracking of the hydride occurs, followed by crack arrest in the more ductile matrix or continued crack growth between hydrides by ductile rupture. Because hydride formation is enhanced by the application of stress, the stress field ahead of the crack tip may induce precipitation of additional hydrides that cleave (ASM Handbook Vol. 13A, 2003).

4.9.7 *Hydrogen trapping* is the mechanism that represents one of the principal factors to determine the hydrogen damage susceptibility of iron-base alloys. This mechanism was widely explained in previous section.

4.10 Hydrogen Damage in Steel

Susceptibility to hydrogen embrittlement of steels under hydrogen-containing atmospheres is affected by many factors. Hydrogen concentrations, metallurgical structure of steel, stress intensity, temperature, environment, and solution composition are the most important factors to determine this susceptibility.

As it was extensively described in previous section, the *concentration of hydrogen* in steel is basically a function of hydrogen-bearing environment pressure, alloy crystal structure, and temperature. Relevant factors that affect the effective pressure hydrogen in the system are the hydrogen gas pressure or pH of the aqueous charging medium in contact with the steel and the environment constituents. In many researches on hydrogen cracking of high-strength steels, it has been demonstrated that small amounts of oxygen in gaseous hydrogen environment can have an inhibitive effect of crack growth.

The action of dissolved ‘poisons’ and their compounds also profoundly affect the rate of absorption of hydrogen into the steel and the recombination reactions. Phosphorous, arsenic, antimony, sulfur, selenium, tellurium, cyanide, and their compounds inhibit the hydrogen recombination reaction in aqueous solutions enhancing the charging of atomic hydrogen into the steel.

The main effect of *microstructural heterogeneities* in steels on stationary hydrogen diffusion at relatively low temperatures is due to the attractive interactions of dissolved hydrogen with the various types of lattice imperfections. In the case of annealed structures of lamellar pearlite or of tempered martensite the internal stresses are decreased, lattice distortions and defects are widely removed and the concentration of carbon atoms is reduced substantially by carbide precipitation. However, carbides size and shape were not analyzed (Riecke et al., 1980). In general, at the same strength level, normalized or bainitic microstructures are less resistant to hydrogen damage than quenched and tempered fine grain steels in which dislocation density is particularly lower.

Recent researches have demonstrated that the most resistant microstructure to hydrogen embrittlement is a highly tempered martensitic structure with equiaxed ferrite grains and spheroidized carbides evenly distributed throughout the matrix (ASM Handbook Vol 13A, 2003). Un-tempered martensite demonstrates poor resistant, specifically to sulfide stress cracking. If the final grain size is greater than prior-austenitic grain size, it produces enhanced resistant; however, it must be larger than the plastic zone size (threshold). It has been found that the carbide/matrix interface is an effective, irreversible trap for hydrogen, capable of dramatically modifying hydrogen transport kinetics. Some studies demonstrate that carbides precipitate preferentially along grain boundaries and dislocations, and that microstructures free of precipitates are virtually embrittled (Stevens et al., 1980).

Non-metallic inclusions and alloying elements have also a profound effect on the hydrogen diffusion, and subsequently on the resistant of steels to hydrogen embrittlement. The hydrogen diffusion coefficient for steel containing elongated sulphide inclusions is higher in the longitudinal direction than in the transversal one. When inclusions are not continuous the coefficient in the longitudinal direction is considerably reduced. Generally, control of common non-metallic impurities (“clean steels”) improves the resistant of steels to hydrogen damage. Additionally, Troiano (1984) states that heterogeneities (traps) generally can improve steel’s susceptibility to hydrogen embrittlement by more uniformly dispersing (not potential crack nuclei) a hydrogen concentration that if localized could accelerate fracture. Clearly, the beneficial nature of such traps will be a strong function of their number and total surface area, their interaction energy with hydrogen, and the hydrogen concentration that must be trapped.

On the other hand, alloying elements and their concentration effects are complicated to explain because a particular alloying element may improve the hydrogen embrittlement resistant or may increase susceptibility to cracking. Molybdenum, for example, is beneficial in increasing the resistant of AISI 4130 steels to sulphide stress cracking (a form of hydrogen stress cracking). The optimum molybdenum content is approximately 0.75 wt% (Garber et al., 1980). However, above this concentration, a separate Mo_2C phase particle in the alloy after tempering at above 500°C (930°F), significantly reducing resistance to sulfide stress cracking.

In general, elements such as C, P, S, Mn, Cr impart greater susceptibility to hydrogen embrittlement in low-carbon steels. Nevertheless, large increases in such element as Cr, Ni, and Mo in order to produce stainless steels alter the crystal structure, microstructure, and subsequently the heat treatment requirements and therefore the hydrogen embrittlement behavior of this group of steels (ASM Handbook Vol. 13A, 2003). Additionally, states that with increasing Cr, Ni, and Mo content, decrease the permeability and diffusivity of hydrogen, and in consequence the susceptibility to hydrogen embrittlement is higher (Elboujdaini *et al*, 2003). Although chromium steel behavior under H₂S environment has not been certainly explored, many researches have demonstrated that chromium steel is highly resistant to CO₂ but poorly resistant to H₂S environments. Silica can be detrimental when segregated to grain boundaries, and beneficial through its indirect role in shifting stage III tempering to higher temperatures and improving the resistance to one-step temper embrittlement (Hirth, 1980). So, microstructure control has been established to be a relevant requirement for limiting the susceptibility of steels to hydrogen embrittlement.

On the other hand, Talbot-Besnard (1982) points that carbon and manganese shift crack tip metal-solution potential towards cathodic values so they increase steel sensitivity. Carbon and nitrogen strengthen grain boundaries and avoid early intergranular failure.

The susceptibility of steels to hydrogen embrittlement is generally enhanced as their strength increase. The *yield strength level* of steel can considerably modify the hydrogen embrittlement susceptibility. Some studies demonstrate that threshold stress intensity for cracking or crack growth of steels (such as AISI 4340 steel in aqueous and gas hydrogen) increases with increasing yield strength. Therefore, very high-strength steels (>100 ksi ~ 700 MPa) should not be used in hydrogen environments due to their threshold stress intensities, which are significantly less than those thresholds under benign conditions. Ultrahigh-strength steels (>200 ksi ~ 1400 MPa) are extremely susceptible to hydrogen embrittlement, even exposed to chlorides-containing solution (principal cause of stress corrosion cracking).

Threshold stress intensity for cracking or crack growth (K_{ISSC} or K_{IH}), below which, for all practical purposes, hydrogen embrittlement cracking does not occur, is also known as stress-intensity value. It is an experimentally determined quantity value that depends on: the nominal strength of the unembrittled component, the amount of hydrogen present in the steel, the location of the hydrogen in the microstructure, and the presence of other embrittling elements or microstructural phases (ASM Handbook Vol. 11, 2002).

Hydrogen embrittlement occurs mainly in high-strength steels commonly utilized in oil and gas industry, however it has been observed in low-strength steels. It occurs principally by loss in tensile ductility or blistering, because hydrogen promotes decohesion of the matrix at inclusion interfaces and carbide particles encouraging the formation and/or growth of voids. Cracking has been also detected in low-strength (low hardness) steels under H₂S-containing environments in the absence of stress.

High-strength (high hardness) steels commonly show an incubation time before fracture initiates under sustained loading. Commonly, this phenomenon occurs in combination with sites of high-stress triaxiality. Fracture initiates internally in the steel, usually at notch roots or under plain strain where triaxial stresses are created. Tensile residual stresses may also promote the initiation of hydrogen stress cracking.

Hydrogen embrittlement is most prevalent near ambient *temperature* (T_{room}), and its tendency decreases with increasing or decreasing temperature. This phenomenon becomes less severe or virtually disappears in steels at higher or lower temperature. Above T_{room} diffusivity of hydrogen is improved and trapping is diminished, while below T_{room} hydrogen motion is very slow to fill enough traps.

4.11 Hydrogen Damage in Pipeline

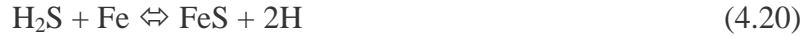
Over half the world's oil and gas reserves are located in environments at great distance from potential users and will require large pipelines (conformed by various joints of pipes) to transport the hydrocarbons to market. During the last thirty years, pipeline design has advanced due to demands for thicker, bigger (diameter), and stronger pipes, and demands on strict dimensional control and accuracy both in diameter and wall thickness.

Generally, small and large diameter pipes are manufactured by a wide range of welding techniques, being submerged arc (single or double side) and electric resistance (high frequency induction) the most common processes; however, smaller diameter pipes can also be seamless. The continuous pipe-production line process uses hot rolled steel coils (rolled steel plates) to form either spiral or longitudinal welded pipes, which later are heat treated and inspected. Hydrogen embrittlement of pipeline steels is a problem to be considered in all pipeline stages: manufacturing, construction, and in-service.

In manufacturing steel plates there are some factors that may create hydrogen-embrittled defects such as hydrogen in molten steel (can be as high as 5 to 8 ppm after refining), center porosity, non-metallic segregations (cracks promoter), and distribution of hydrogen in the thickness direction of the previous steel ingot. The primary source of hydrogen in steelmaking is moisture in the atmosphere and in the additives. Nevertheless, effective hot rolling technique and dehydrogenation process may eliminate internal hydrogen-induced defects and make possible a almost free-internal-defect pipe.

Pipeline carrying wet sour hydrocarbons can develop hydrogen embrittlement of the pipe steel. In the absence of stress, pipeline steels exposed to sour fluids experience longitudinal cracks through the pipe wall, and the tip of one crack may converge with another in 'stepwise' pattern (stepwise cracking). The most common form of atomic hydrogen available at the internal surface of pipeline is usually from the oxygen-accelerated dissociation of H_2S gas molecule in the presence of water. The fugacity of hydrogen generated during sulfide corrosion is extremely high.

In general, hydrogen-induced cracking mechanism of high-strength pipeline steels in contact with a wet H₂S-containing environment can be explained by the corrosion reaction



under a combined action of corrosion and tensile stress. This chemical reaction produces FeS that represents a permeated layer by atomic hydrogen diffusing to favorable sites where molecular hydrogen is formed. Zhao *et al* (2003) states that a continuous FeS adherent scale produced on the surface of the steel will protect the metal against further attack. However, under the imposed aqueous H₂S environments, the FeS scale does not avoid hydrogen penetration into the plastic region of the crack tip, because the adherent strength between the FeS scale and the matrix is weak and the FeS scale is apt to fall off. Also, there are numerous microcracks and corrosion grooves distributed on the surface of corrosion scales and crystal granules of FeS. Moreover, FeS acts as a cathode to form a active battery with the matrix. All these are more helpful to both the above corrosion reaction and the followed hydrogen penetration.

When the hydrogen is cathodically evolved in the surface of the steel, H₂S tends to cause hydrogen atoms to enter the steel rather than to leave the steel. In the steel, hydrogen atoms tend to diffuse to those sites with high triaxial tensile stress or some microstructural defects such as coarsening carbides, inclusions, and segregations. When the hydrogen accumulation in these sites is increased up to a critical value, hydrogen embrittlement can occur.

In addition, hydrogen penetration may be directly related to a pseudo-stress imposed in the material. When this pseudo-stress is imposed, the highly localized stress may induce hydrogen enrichment. The hydrogen concentration by the localized stress can be described by

$$C_H = C_0 e^{(\sigma_h V_H / RT)} \quad (4.21)$$

where C_0 , σ_h , and V_H are the hydrogen concentration average, the hydrostatic stress and the partial molar volume of hydrogen, respectively. When C_H reaches the critical value, cracking occurs.

Hydrogen-induced degradation in pipeline steels generally takes a form of hydrogen-induced blister cracking (HIBC), which is induced by hydrogen trapped at interfaces between matrix and, typically, hot roll-flattened manganese sulfide inclusions. An externally applied stress influences considerably the manner of HIBC extension; in the absence of external stress HIBC develops by ‘stepwise’ linking of internal blister along with considerable plastic deformation. Under externally applied stress the HIBC

develops by linking blisters formed perpendicular to the applied stress (Oriani *et al*, 1985).

Elongated sulfide inclusions, such as type II MnS, and glassy silicates are particularly favorable sites for the formation of molecular hydrogen in the steel. Lower volume fractions of inclusions corresponded to higher resistance to hydrogen damage. The hydrogen trapped principally at elongated MnS inclusions are responsible for hydrogen-induced cracking due to either internal pressure or decohesion of the inclusion-matrix interface. However, ellipsoidal sulfides inclusions, such as type I MnS, have better hydrogen-induced cracking resistance. Atomic hydrogen is also available from other sources such as cathodic protection and aqueous environments.

A flat inclusion-matrix interface will accelerate stress-induced hydrogen diffusion into the crack tip region, when it is separated and pressurized with hydrogen gas to form a crack. Around a global or ellipsoidal inclusion, on the other hand, no stress-induced diffusion takes place because the lack of triaxial stresses concentration. In consequence, inclusion shape control is essential for improvement hydrogen damage resistance of pipeline steels (Oriani *et al*, 1985).

Non-metallic inclusions act as hydrogen traps and offer low resistant to hydrogen embrittlement. Once hydrogen is trapped at an inclusion, it may achieve a high internal pressure, reducing as well the interatomic cohesive forces and surface energy at the inclusion surface ($\sigma_C^H < \sigma_C^o$). This phenomenon significantly affects the dislocation motion in the plastic zone. This theory is schematically illustrated in Fig. 5.

A crack will be initiated or assisted when the sum of all applied (σ_a^H) and residual (σ_r^H) stresses is greater than the cohesive strength (σ_C^H). The amount of hydrogen trapped on the inclusion and the specific quantity of hydrogen trapped at which a crack will be induced by hydrogen depend on various inclusion parameters: shape, size, distribution, density, neighboring structure and impurities (which reduce inclusion-matrix interface cohesion strength).

As report previously, pipeline steel microstructure also play an important role in hydrogen embrittlement resistance. Elboudjaini *et al* (2003) reports that heavily banded microstructures could enhance hydrogen-induced cracking by providing low fracture resistance paths for cracks to propagate more easily. However, Serna *et al* (2003) states that banded structure presented by microalloyed steels may contribute to increase hydrogen damage resistant at atmospheric conditions.

In ferritic pipeline steels, bainite and un-tempered martensite are the most susceptible microstructures whereas quenched-tempered and normalized are the most resistant to hydrogen embrittlement. In other words, many studies have demonstrated that the microstructure after normalizing, i.e. fine ferrite-pearlite structure, and after quench and temper treatment, i.e. tempered martensite, of different pipeline steel grades (up to X62) reduces hydrogen-induced cracking susceptibility.

However, Zhao *et al* (2003), studying three common pipeline steel microstructures, defines the acicular ferrite-dominated structure as the optimum candidate microstructure for oil and gas pipeline steels in sour service, while ultra fine ferrite microstructure is in second position. The ferrite-pearlite microstructure possesses the worst hydrogen embrittlement (sulfide stress cracking) resistance because since carbides and MnS inclusions precipitates along the banded pearlite, hydrogen diffuses to their interfaces reaching the critical hydrogen concentration.

From pipeline steelmaking process, sulfur represent an impurity while copper, manganese, and nickel are commonly added alloying elements. Lowering the sulfur content and increasing copper content is beneficial due to sulfur ‘poison’ behavior and Cu-based protective and impermeable surface film. Addition of 0.3 %wt Cu is known to improve hydrogen-induced cracking resistant of pipeline steels, but this beneficial effect prevails only in environments with relatively high pH (5 or more) and diminishes in low-pH (3.5 or less) (ASM Handbook Vol. 11, 2002).

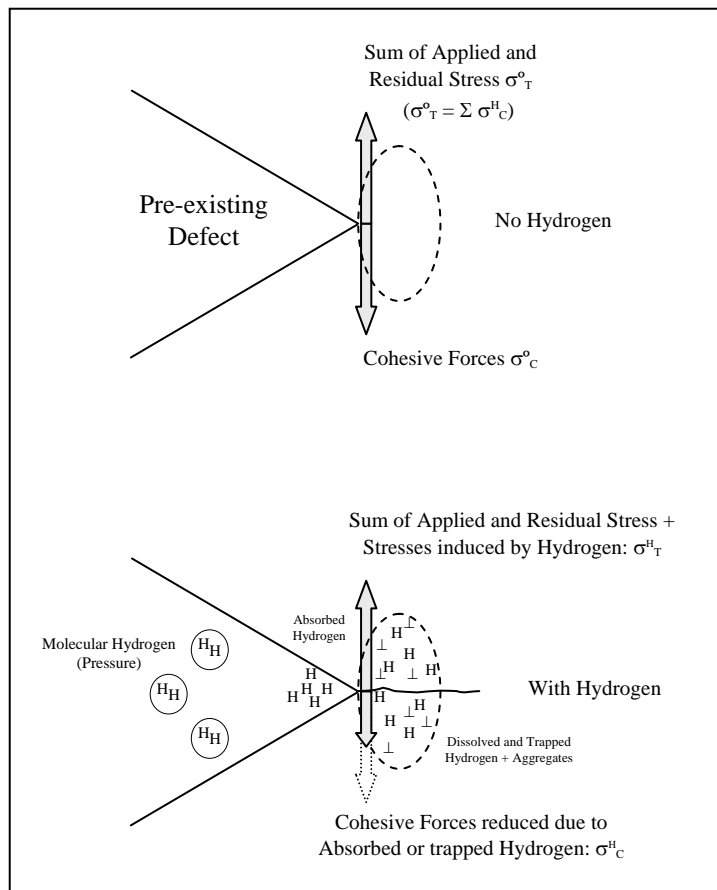


Fig. 5. Effects of hydrogen on preexisting defects.

4.13 Hydrogen Embrittlement of Cathodic Protected Steels

Hydrogen diffusion into iron and steel is strongly affected by various electrochemical and environmental factors; typically, it increases with cathodic polarization. Pipelines are commonly cathodically protected either with sacrificial anodes or impressed current. Although the cathodic protection of such tubulars usually does not cause hydrogen embrittlement, high-strength steel can be embrittled by cathodic protection. Nevertheless, experiments using relative low-strength pipeline steel demonstrate that at considerably large (more negative) cathodic current density (“overprotection”) steel ductility can be reduced. Since excessive cathodic protection would result in undesirable hydrogen evolution, the lack of steel ductility is considered to be the result of hydrogen degradation due to cathodically evolved hydrogen at crack tips and pipe surfaces. If pipeline is additionally protected with external coating, overprotection currents generate electrochemically hydrogen atoms on coating defects such as “holidays.” The pipeline material can absorb those atoms enhancing hydrogen-induced cracking.

Cathodic protection reduces the corrosion rate by cathodic polarization of a corroding pipeline steel surface. Cathodic polarization reduces the rate of the half-cell reaction



with an excess of electrons, which also increases the rate of oxygen reduction and OH^{-} production by the reaction (Jones, 1996)



Sometime a rectifier is used to supply impressed current for cathodic polarization of the pipeline steel. Since this mechanism of protection depends on external current polarizing cathodic elements of local half-cells to the open-circuit potential of the anodes, at specific time the cathode and anode potentials on the pipeline surface become equal and corrosion currents no longer flow. Consequently there is no tendency for metal ions to enter into solution (Das *et al*, 1977). However, in the extreme case of overprotection copious evolution of hydrogen atoms occurs at the pipe surface by the reduction of dissolved oxygen. The amount of evolved hydrogen generated by overprotection increases as a function of applied polarization potential and time, and could be partially absorbed by the steel leading to catastrophic failures as a result of hydrogen embrittlement. The concentration of hydrogen at the pipe surface is also dependent of hydrogen entry and effusion, and the surface features; for instance, oxides and scales present on the surface. Moreover, the hydrogen gradient in the metal matrix depends on the loading time, the diffusion rate, and the possibility for the hydrogen to escape (Olsen *et al*, 2001).

Considering high-strength steel pipelines in aqueous environment, cathodic polarization, which promotes the evolution of hydrogen at the steel surface, causes an increase in crack growth rate while anodic polarization, which stimulates corrosion, decreases the crack growth rate at low pH values but increases it at high pH values (Oriani *et al*, 1985). An increase in hydrogen uptake (“hydrogen entry or diffusion”) and in hydrogen embrittlement at low anodic polarization was observed for high-strength low-alloy steels in NaCl solutions and low-carbon steels in carbonate/bicarbonate solutions. High hydrogen uptake may occur within occluded cells, such as cracks, pits, and crevices, when the external surface of the steel is anodically polarized. At anodic potentials, hydrogen evolution in the occluded cells results from a shift of a potential in the negative direction due to the ohmic potential drop, so that the thermodynamic conditions for the hydrogen evolution are attained (Flis and Zakroczymski, 1992).

Currently, martensitic stainless steels, such as Super 13%Cr (average composition: 13%wt Cr, 4%wt Ni, and 1.5%wt Mo), are made readily weldable and represent a qualified alternative for materials in pipelines frequently used in subsea applications. In general, the weldments are made by mechanized pulsed GMAW using duplex stainless steel (softer alloy) as consumable (filler material). Olsen *et al* (2001) demonstrates that, under cathodic polarization (-1050 mV-SCE), hydrogen-induced cracks initiate in the weld metal (martensitic SS) and propagate through the softer-filler alloy (duplex SS), which exhibit better resistance to hydrogen embrittlement.

The crack-tip opening displacement (CTOD) test is a method that covers the determination of critical CTOD values at one or more of several crack extension events. CTOD values can be used as measures of fracture toughness for metallic materials, and are especially appropriate to materials that exhibit a change from ductile to brittle behavior with decreasing temperature (ASTM E1290, 2002). CTOD testing can evaluate critical CTOD (δ_c), which gives the maximum tolerable defect size of materials. Some studies show that the possibility of hydrogen-induced cracking in pipelines could be very small when the surfaces are smooth. However, a fracture toughness-based investigation demonstrate that the critical displacement δ_c of line pipe steels under cathodic protection decreases with a decrease in the steel’s stress-intensity-factor, and it is deeply dependent on cathodic current density above threshold current values. In consequence, hydrogen-induced cracking in pipelines under cathodic protection can be define as a function of surface mechanical conditions (such as defect size), and the characteristics of the cathodic current. In order to prevent initiation of hydrogen-induced cracking at surface defects in pipeline under cathodic protection, inspection of casting and surface defects, evaluation of applied stresses, current and the critical CTOD with cathodic protection are the methods that may be adopted (Hagiwara and Meyer, 2000).

4.14 Hydrogen Effect on Magnetic Properties of Steel

The behavior of hydrogen in ferromagnetic materials has been studied by a very sensitive method called *magnetic aftereffect*. When a magnetic field near a hydrogen-

charged ferromagnetic material is abruptly changed a redistribution of hydrogen atoms occurs. Those atoms diffuse to energetically more favorable sides inside the magnetic domain walls. This phenomenon gives rise to relaxation of the magnetic reluctance. The characteristic time for this *aftereffect* is related to the diffusion coefficient of hydrogen.

An interstitial alloy is an alloy formed when some of the interstices or holes in the densely packed host metal structure (tetrahedral or octahedral spaces between the atoms) are occupied by small atoms of non-metallic elements such as H, C, N, and B. When interstitial atoms are located in tetrahedral positions they are surrounded by four atoms, and six atoms when they are located in octahedral positions.

The number of interstitial atoms that are actually accommodated in the structure is much less than the available interstitial sites. Introducing a metalloid atom into a interstitial position leads to lattice distortions, since the atom requires more place than is offered by the interstitial void. A chemical binding phenomenon also takes place between the metal and the metalloid atoms. It is caused by the distribution of the electrons of the metalloid atoms to the 3d-band of the host metal. In general, the hydrogen concentration in many transition metal alloys depends of the magnetic properties of the metal, basically, because of the number of outer electrons per constituent atom.

The electrons on the interstitial hydrogen atoms are essentially contributed to the d-band of iron and its alloys. The increase in the valence electron concentration and the lattice expansion cause changes in the magnetic properties. These alterations appear to be almost equivalent to the change that would occur if the electron concentration of the metal were changed by substitutional alloying. The alloys with higher electron concentrations are strong ferromagnets, while those with lower electron concentrations are alloys with strong volume dependent magnetic properties (Pepperhoff and Acet, 2001). Each alloy has its own ability to have its hydrogen solubility altered by a magnetic field.

As it is known, αFe has a ferromagnetic nature and γFe has an antiferromagnetic ground state, while the ground state of εFe is nonmagnetic. This hexagonal ε -phase has strong atomic volume dependent magnetic properties. The lattice expansion and the ferromagnetism of $\varepsilon\text{Fe-H}$ are interrelated. Although εFe is nonmagnetic in the ground state, it is antiferromagnetic at larger volumes with a volume dependent magnetic moment. Still, at larger volumes than that corresponding to the antiferromagnetic state, it becomes ferromagnetic with larger magnetic moment. The presence of ferromagnetism in $\text{FeH}_{0.7}$ (hydrogen solubility of 0.7 in Fe-H system) and the volume dependence of its magnetic moment are observed experimentally and predicted in theoretical calculations. The reason for the large volume of $\text{FeH}_{0.7}$ is its ferromagnetism. However, it must also be taken in account that hydrogen donates its electron to the d-band and influences the banding conditions. Since hydrogen strongly influences the physical properties of 3d-metals, the concentration dependence of the magnetic properties of the metal-hydrogen system can be based on a simple band model, and with it, predictions can be made on the properties of the less investigated metal-hydrogen system (Pepperhoff and Acet, 2001).

Since hydrogen atoms donate their electrons to the d-band of transition metal, these bestowed electrons modify electron spin configuration and, in consequence, the material behavior under a magnetic field. This phenomenon varies the entropy of the system resulting in a variation of the external work. The diffusible hydrogen content can be related to magnetism from two different definitions of the Gibbs free energy based on chemical equilibrium and electrochemical equilibrium. The change in Gibbs free energy associated with a chemical reaction ($\text{H}_2 \rightleftharpoons 2\text{H}$) is a useful indicator of whether the reaction will proceed spontaneously. Since the change in free energy is equal to the maximum useful work which can be accomplished by the reaction

$$\Delta G = -w_{\max} \quad (4.24)$$

then a negative ΔG associated with a reaction indicates that it can happen spontaneously. For a chemical equilibrium, in which there is not a external work, the change of Gibbs free energy is zero. On the other hand, for electrochemical equilibrium, the free-energy change corresponds to a electrical charge (nF) taken reversibly at equilibrium through a electrochemical potential (E):

$$\Delta G = -nFE. \quad (4.25)$$

where ' nFE ' represents the external work with n equal to the number of electrons (or equivalents) exchanged in the reaction, and F as the Faraday's constant (96,500 coulombs/equivalents). For the $\text{H}_2 \rightleftharpoons 2\text{H}$ reaction, the free-energy change becomes:

$$\Delta G = \Delta G^\circ + RT \ln ([\text{H}]^2 / P_{\text{H}_2}) \quad (4.26)$$

where ΔG° is the standard-state free energy change for the hydrogen reduction reaction, R is the gas constant, T is absolute temperature, $[\text{H}]$ the equilibrium hydrogen content in solid solution, and P_{H_2} is the partial pressure of hydrogen in the system. ΔG° for a reaction can be calculated from tabulated standard-state free energy data.

From chapter two, the work experienced by a material under a magnetic field can be define by potential energy. Relating the potential energy with the Gibbs free energy, it becomes

$$\Delta G = \Delta M H \quad (4.27)$$

where ΔM is the change in magnetization and H is the magnetic field. For the hydrogen reduction reaction:

$$\Delta M H = \Delta G^\circ + RT \ln ([H]^2 / P_{H_2}) \quad (4.28)$$

This thermodynamic description is based on derivations of the definitions of enthalpy, entropy, Gibbs free-energy, and external work, as well as the isothermal and isobaric conditions of the system. After rearrangements of the equation 4.31, it becomes

$$(H\Delta M / RT) - (\Delta G^\circ / RT) = \ln ([H]^2 / P_{H_2})$$

where $\Delta G^\circ / RT$ can be considered as a constant term (C). Therefore, the concentration of diffusible hydrogen in the metal is given by

$$[H] = P_{H_2}^{1/2} * \exp \left[\frac{H\Delta M}{RT} - C \right] \quad (4.29)$$

where P_{H_2} may be considered 1 ($P_{H_2}=1\text{atm}$). As hydrogen concentration is exponentially related to the magnetic field, this theoretical description conceptually suggests that the diffusible hydrogen content in pipeline steels must be significantly affected by the magnetization produced during pigging operations. In other words, small changes of magnetization undoubtedly may cause large changes in hydrogen content. The fundamental link between magnetism and the hydrogen solubility in high strength pipeline steels will be the principal subject of this work.

Attachment # 2

Experimental Plan and Procedures

CHAPTER 5

EXPERIMENT PLAN AND PROCEDURE

5.1 Introduction

Pipelines in the Beaufort Sea (Alaska) utilize high strength steel grades such as API Spec. 5L Grade X52 and X70, therefore, initial experimentation was planned with these steel grades and samples were obtained for analysis. The preliminary samples were obtained from a local energy company. Even though the wall thicknesses are thinner than those used in Alaska, the initial investigation with the thinner gage material will be beneficial in setting up the experimental procedure with the actual thick gage steel.

To ascertain the material characteristics, set of tests was run to verify the mechanical properties and the chemical composition of the steels. The tests are performed according to API Spec5L testing procedure. Microstructural analysis was required to complete the characterization of the received material.

For the experiments, both electrochemical techniques Devanathan-Stachurski cell and Barnacle electrode were employed to determine the rate of permeation of electrolytic hydrogen and the diffusion or mobile hydrogen concentration. The standard practice ASTM G148 and the standard test method ASTM F1113 are used to perform these techniques, respectively.

To achieve the primary end focus of this project a magnetic field device is designed according to Biot-Savart law. This fundamental law of electromagnetism allows the calculation of the strength of a magnetic field that is produced by an electrical current. The magnetic field must be strong enough to produce the saturation magnetic flux density commonly used in pipeline steels.

5.2 Material Characterization

5.2.1 Tensile Test

Four standard size tensile test specimens from large-diameter tubular products are cut from both steel pipes; two specimens from each steel grade, X52 and X70. The tensile tests were run according to the API Spec 5L requirements. Table 5.1 shows the mechanical properties of the steel tested (Figure 5.1) in this study, and the properties of the specified steel as per API Spec. 5L requirements.

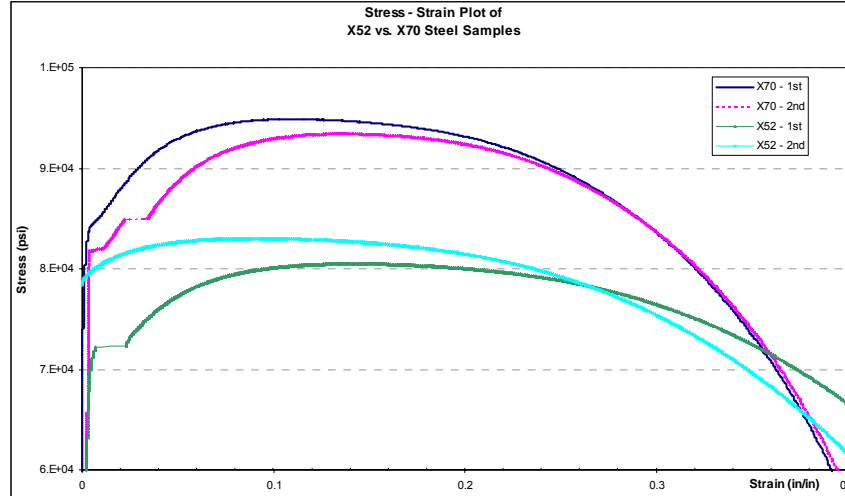


Figure 5.1. Tensile test diagram of tested steel, X52 and X70.

Table 5.1. Mechanical properties of tested steel, X52 and X70.

Sample	API Spec. 5L Requirements		Tensile Test	
	Yield Strength Minimum (psi)	UTS Minimum (psi)	Yield Strength (psi)	UTS (psi)
X52 – a	52,000	66,000	78,998	80,523
X52 – b			72,227	83,020
X70 – a	70,000	82,000	81,892	94,893
X70 – b			83,346	93,429

5.2.2 Microstructure and Chemical Composition

The microstructures of all the samples were examined using standard optical microscopy, where typical photomicrographs are shown in Figure 5.2. The X52 pipeline steel sample exhibited equiaxed ferrite/low-pearlite microstructure typical of heat-treated, microalloyed steels with grain sizes ranging from 4 to 20 μm (Fig. 5.2 a-b). The X70 pipeline steel sample also displayed a ferrite/low-pearlite microstructure but with slightly more refined grain sizes ranging from 3 to 12 μm (Fig. 5.2 c-d). The elongated nature of the grains reflecting the rolling direction and texturing are evident in these micrographs.

The steel samples used for the laboratory tests were low carbon steel, produced according to API 5L Grade X52 and X70 specifications. Table 5.2 shows the chemical composition of the steel tested in this study, and for the steel matching the API Spec. 5L requirements.

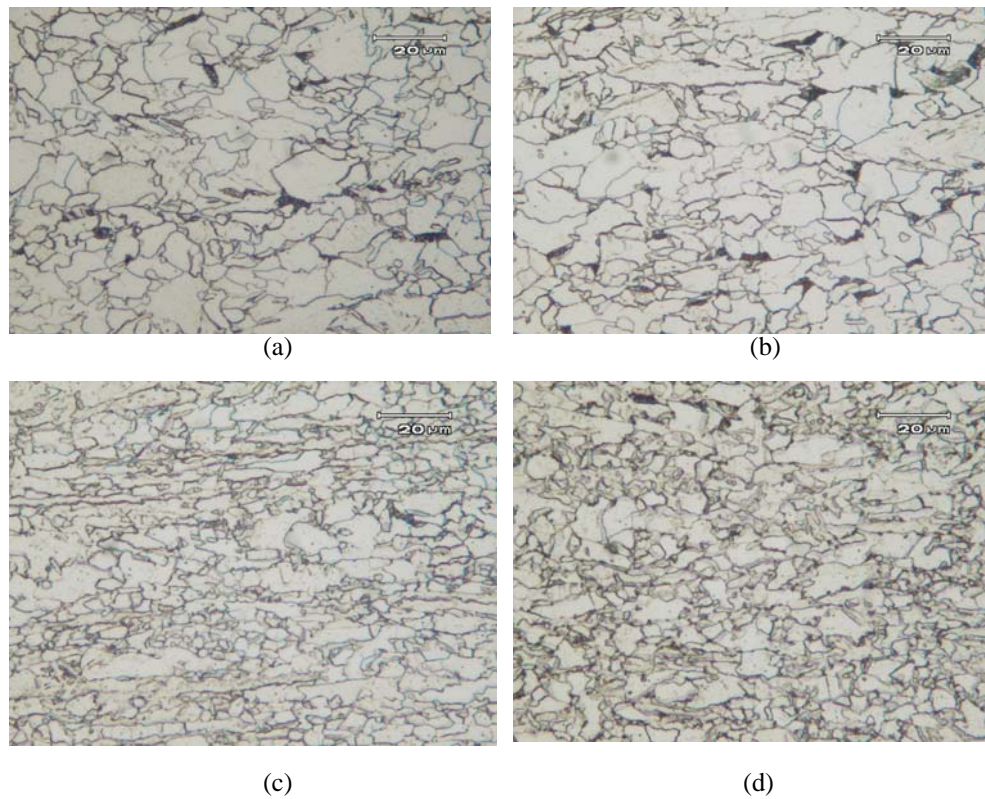


Figure 5.2. Microphotography of both X52 (a-b) and X70 (c-d) steel samples showing a ferrite/pearlite microstructure. (a-c) Longitudinal sections. (b-d) Transversal sections.

Table 5.2. Chemical Composition of tested steel, X52 and X70.

<i>Material</i>	<i>Carbon (%)</i>	<i>Manganese (%)</i>	<i>Phosphorus (%)</i>	<i>Sulfur (%)</i>
X52 Tested Steel	0.0610	1.31	0.005	0.0069
	0.0609	1.30	0.004	0.0069
	0.0606	1.31	0.005	0.0073
X70 Tested Steel	0.0740	1.41	0.012	0.0029
	0.0655	1.41	0.005	0.0033
	0.0718	1.42	0.012	0.0031
API X52	0.30 max.	1.35 max.	0.04 max.	0.05 max.
API X70	0.23 max.	1.60 max.	0.04 max.	0.05 max.

5.3 Devanathan-Stachurski Permeation Cell – Experimental Procedure

a. *Objective*

The Devanathan-Stachurski electrochemical cell has been developed to measure the instantaneous rate of permeation of electrolytic hydrogen through membranes of materials, based on the theory that the rate of permeation of hydrogen is controlled by diffusion in the material.

This document gives a procedure for the evaluation of the concentration of hydrogen absorbed, and hydrogen permeation and transport in metals. It can be applied, in principle, to all metals and alloys which have a high solubility for hydrogen, and for which hydrogen permeation is measurable.

This procedure can be used to evaluate the severity of hydrogen charging produced by diverse sources (corrosive environments and cathodic polarization) and to determine the effect of processing, metallurgical, and environmental variables, as well as properties of materials on diffusion of hydrogen in metals.

b. *Principle*

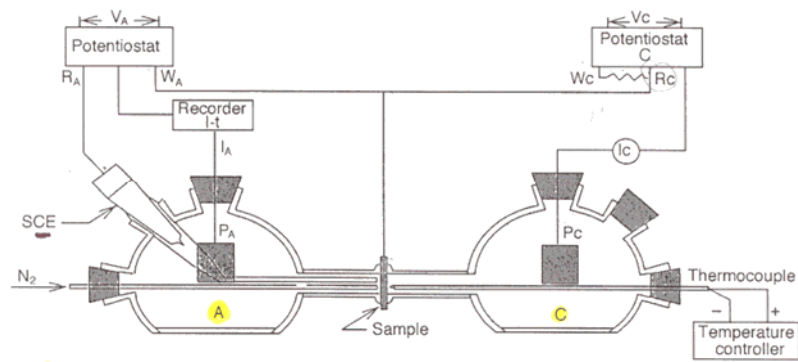
The principle of the Devanathan-Stachurski cell, based on an electrochemical technique, utilizes a metallic membrane forming the partition wall between the two compartments of twin electrochemical cells with electrodes each one (Fig. 1). One side of the membrane is coverage with absorbed atomic hydrogen produced by cathodic reduction at a certain fixed level, while on the opposite side the amount of atomic hydrogen should be always zero. The membrane must be coated with palladium on the oxidizing side to search zero hydrogen concentration. The opposite compartment contains an alkaline electrolyte in which the membrane surface is kept passive at a potential, high enough to oxidize by anodic polarization (potentiostatic circuit) any hydrogen coming through the membrane. The current in the anodic potentiostatic circuit is by Faraday's laws a direct measurement of the instantaneous rate of permeation of hydrogen.

c. *Apparatus and Test Environment*

The Devanathan-Stachurski cell (Fig. 5.3) consists of two identical electrochemical units terminating in standard half-inch pipe flanges, a charging or cathodic unit, and an oxidation cell or anodic unit. Each flange holds a Teflon O-ring facing the membrane polished flat. The assembly is jointed with the membrane in between the O-rings. The electrodes in each compartment are a bright platinum auxiliary and a Luggin capillary-calomel reference.

The cathodic unit is filled with 1 liter of a solution of 0.2N acetic acid - 0.1N sodium acetate, and a constant current density of 50 mA/cm² (500 A/m²) was

applied to the cathodic surface of the specimen. The anodic unit is filled with 1 liter of a solution of 0.1N sodium hydroxide, and a constant voltage of 50 mV_{SCE} was applied to force the hydrogen concentration on the surface to zero. Both solutions are previously electrolyzed for 24 hrs in an external cell and deaerated by pure argon right before the test. Deoxygenated nitrogen is injected into the outlet compartment to promote storing. A platinum coating is applied on the exit surface of the membrane to moreover ensure zero hydrogen concentration.



Schematic Diagram (Yen, S.K., et al.)

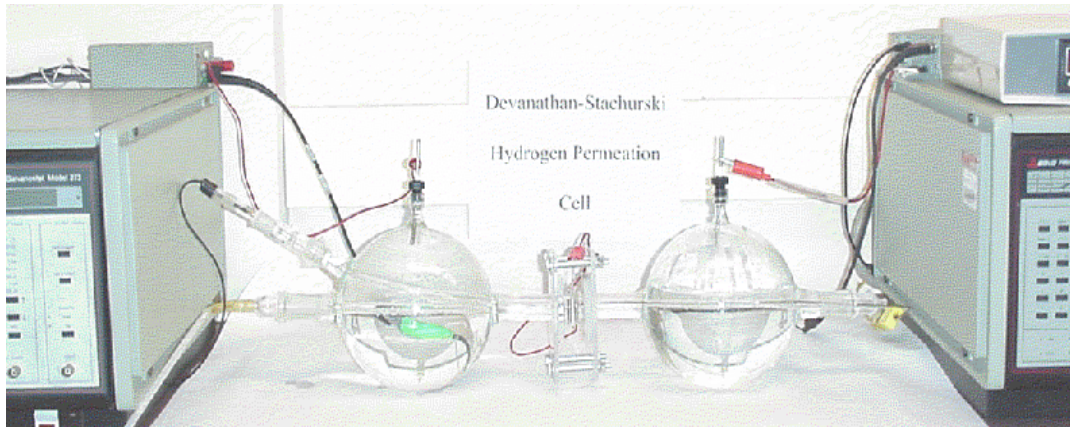


Figure 5.3. Hydrogen Permeation cell (Devanathan-Stachurski) and schematic diagram. C: cathodic unit. A: anodic unit. P_C-P_A: auxiliary platinum electrodes. R_C-R_A: reference P_C electrodes. W_C-W_A: working electrodes.

Chemical Solutions

Cathodic Unit: 1 liter of 0.2N acetic acid (CH₃COOH) - 0.1N sodium acetate (CH₃COONa) solution.

- *0.2N CH₃COOH*

1M = mass/L / GFW (gram formula weight)

1N = 1M * Z

Bases: Z is simply the number of protons that will be donated.

Acid: Z is the number of hydroxide ions liberated

1M = mass/L / (12+3+12+16+16+1) = mass/L / 60

1N = 1M * Z (acetic acid=1 / CH₃COOH → CH₃COO⁻ + H⁺) = mass/L / 60

Concentration: 60 gr./L (1N) 0.2N = 0.2 * 1N = 12

Final Concentration *0.2N CH₃COOH* = 12gr/L

- *0.1N CH₃COONa*

1M = mass/L / (12+3+12+16+16+1+23) = mass/L / 83

1N = 1M * Z (=1) = mass/L / 83

Concentration: 83 gr./L

0.2N = 0.2 * 1N

Final Concentration *0.2N CH₃COOH* = 16.6gr/L

Anodic Unit: 1 liter of 0.1N sodium hydroxide (NaOH) solution.

- *0.1N NaOH*

1M = mass/L / (23+16+1) = mass/L / 40

1N = 1M * Z (=1) = mass/L / 40

Concentration: 40 gr./L

0.1N = 0.1 * 1N

Concentration *0.1M NaOH* = 4gr/L

Temperature

The temperature of the solution has a considerably effect on hydrogen permeation. To carry out all measurements under temperature controlled conditions the cell is thermostatically controlled at room temperature (69 ±2°F) for the period of the experiment.

d. *Specimens*

The specimens used in this study are 1.60-mm (0.063-in) thick, flat, long transverse, double-notched tensile plate of pipeline steels (API Grade X52 and X70), finished by surface grinding. The specimens must be cleaned in non-chlorinated solvents to removes traces of chemicals and degreased before experiment.

e. *Test Procedure*

Based on ASTM G148-97 “Standard Practice for Evaluation of Hydrogen Uptake, Permeation, and transport in Metals by an Electrochemical Technique.”

f. *Environmental Control and Monitoring*

Based on ASTM G148-97 “Standard Practice for Evaluation of Hydrogen Uptake, Permeation, and transport in Metals by an Electrochemical Technique.”

g. *Procedures for Analysis of Results*

Based on ASTM G148-97 “Standard Practice for Evaluation of Hydrogen Uptake, Permeation, and transport in Metals by an Electrochemical Technique.”

h. *Reporting.*

Based on ASTM G148-97 “Standard Practice for Evaluation of Hydrogen Uptake, Permeation, and transport in Metals by an Electrochemical Technique.” In addition, a record of the diffusion coefficient values plotting D_{eff} vs. magnetic field is required.

5.4 Barnacle Electrode Method – Experimental Procedure

a. *Objective*

The barnacle electrode method has been developed basically to determine mobile hydrogen concentration under service environments and to correlate hydrogen concentration with delayed failure in materials such as high-strength steels.

b. *Principle*

The principle of the barnacle electrode method is based on the electrochemical technique used in the Devanathan Permeation Cell. The barnacle electrode method essentially makes use of the extraction side of the Devanathan cell and requires that the sample be previously charged with a uniform known distribution of hydrogen throughout.

c. *Apparatus and Test Environment*

The barnacle electrode method consists of a steel sample as the anode, a nickel/nickel oxide (Ni/NiO) electrode as the cathode, a Teflon block that has two circular opening, and a clamp frame. Sodium hydroxide solution, 0.2 M, is used to fill the cell for measurements (ASTM F1113-87 “Standard Test Method for Electrochemical Measurement of Diffusible Hydrogen in Steels”).

Based on the hydrogen content within the steel, the electrochemical potential difference between the steel sample and the Ni/NiO electrode should be on the order of 750 – 850 mV. Notice that the fully charged Ni/NiO electrode is 310 mV noble to the saturated calomel electrode in sodium solution.

Chemical Solutions

- *0.2M NaOH*
1M = mass/L / (23+16+1) = mass/L / 40
Concentration: 40 gr/L
0.2M = 0.2 * 1M
Final Concentration *0.2M NaOH* = 8gr/L

Temperature

The temperature of the solution has a considerably effect on hydrogen permeation. To carry out all measurements under temperature controlled conditions the solution is thermostatically controlled at room temperature (69 ±2°F) for the period of the experiment.

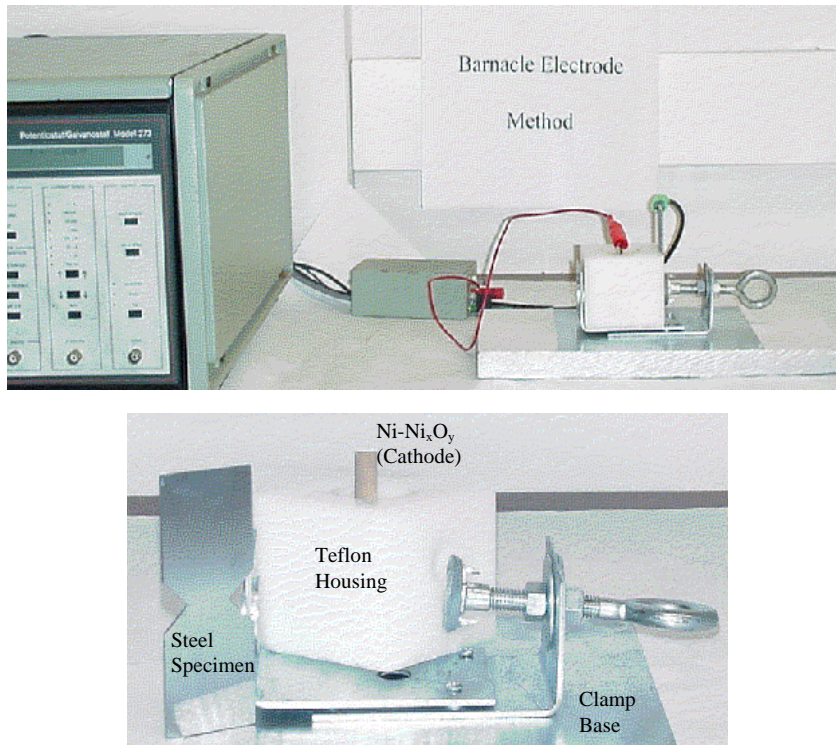


Figure 5.4 Barnacle Electrode Method.

d. Specimens

The specimens used in this study are 1.60-mm (0.063-in) thick, flat, long transverse, double-notched tensile plate of pipeline steels (API Grade X52 and X70), finished by surface grinding.

e. Procedure

Based on ASTM F1113-87 “Standard Test Method for Electrochemical Measurement of Diffusible Hydrogen in Steels”.

f. Calibration and Standardization

Based on ASTM F1113-87 “Standard Test Method for Electrochemical Measurement of Diffusible Hydrogen in Steels”.

g. Calculations and Interpretation of Results

Based on ASTM F1113-87 “Standard Test Method for Electrochemical Measurement of Diffusible Hydrogen in Steels”.

h. Reporting.

Based on ASTM F1113-87 “Standard Test Method for Electrochemical Measurement of Diffusible Hydrogen in Steels”. In addition, a record of the diffusion coefficient values plotting D_{eff} vs. magnetic field is required.

i. Initial Hydrogen Concentration Determination (Cathodic Charging)

To establish the initial hydrogen concentration, a 12-specimen set was sliced from both steel samples API 5L X52 and X70 into 0.30 - 0.55 cm²-area samples. The samples were subsequently washed with acetone for 5 min., baked at 400°C for 1 hr., and mounted on epoxy resin to reduce galvanic cell effect in the Hydrogen-Charging System and to ensure complete submerging of the charged area into the solution. The uncharged hydrogen concentration was determined with a 2-specimen set using the LECO-Hydrogen Determinator RH-404. The mounted samples (10-specimen set), which are electrically connected to the power supplier through a copper wire, were surface finished until a 'bench grinder' finishing was obtained.

The cathodic charging was carried out electrolytically always in a new solution of 10% H₂SO₄ and 100 mg/L NaAsO₄ using a platinum wire as cathode and the steel sample as the anode. Both the temperature (T_{room}) and the pH (up to 0.4 at $t = 0$) of the solution were continuously monitored, and the DC power supply was fixed at 5.0 volts during the charging period. The 10-specimen set of both steels was charged at fixed time intervals of 1, 2, 4, 6, and 8 hrs to establish the optimum hydrogen concentration (C_0) and charging time $t_{(C_0)}$. The schematic diagram of the cathodic charging apparatus is as follow:

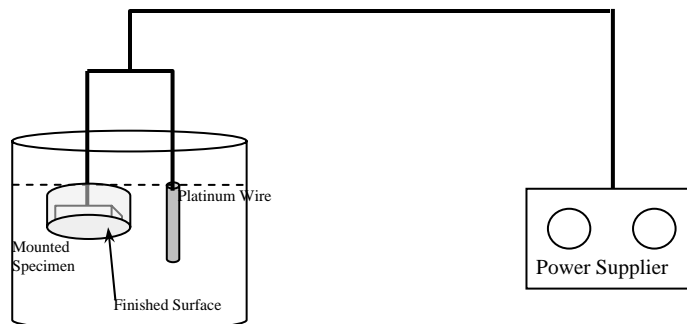


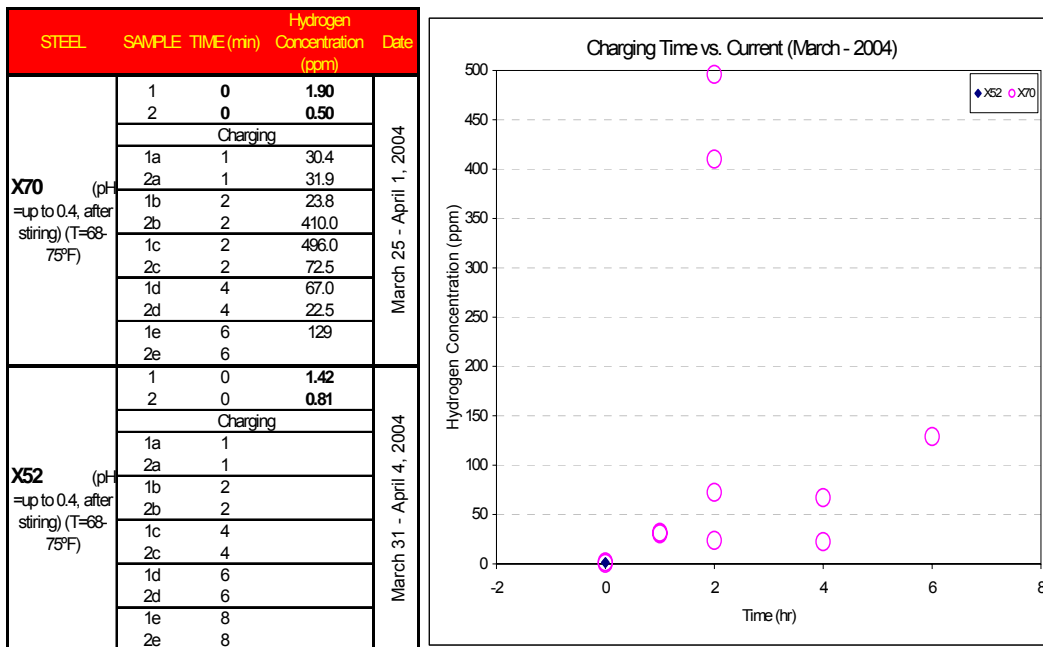
Figure 5.5 Schematic diagram of hydrogen cathodic charging apparatus.

The exposed area and the weight of each sample were recorded as well as the pH of the solution and the achieved hydrogen concentration. The results are plotted in a hydrogen concentration vs. time chart. Previous results have already been obtained for both X52 and X70 steels.

Table 5.3. Hydrogen Cathodic Charging Test results.

STEEL	SAMPLE #	CHANGING TIME (HR)	AREA (cm ²) / WEIGHT (gr.)	HYDROGEN CONCENTRATION (ppm)	pH (max.)	VOLTAGE (volt)
X70	1a	--No--	---	1.9		---
	2a	--No--	---	0.5		---
	2a	1	0.453 / 1.084	30.4	0.4	5.0
	2b	1	0.453 / 0.849	31.9	0.4	5.0
	3a	2	0.377 / 0.687	23.8	0.4	5.0
	3b	2	0.392 / 0.809	410.0	0.4	5.0
	3a	2	0.339 / 1.154	496.0	0.4	5.0
	3b	2	0.471 / 0.735	72.5	0.4	5.0
	4a	4	0.503 / 1.054	67.0	0.4	5.0
	4b	4	0.403 / 0.953	22.5	0.4	5.0
	5a	6	0.378 / -38%	129.0	0.4	5.0
	5b	6				
6a	8					
6b	8					
X52	1a	--No--	---	1.42		---
	2a	--No--	---	0.81		---
	2a	1				5.0
	2b	1				5.0
	3a	2				5.0
	3b	2				5.0
	4a	4				5.0
	4b	4				5.0
	5a	6				5.0
	5b	6				5.0
	6a	8				5.0
	6b	8				5.0

Table 5.4. Hydrogen Concentration in both X52 and X70 steels. C_H versus charging time plot.



5.5 Magnetic Properties

The magnetizing system of the Magnetic Flux Leakage (MFL) tool creates a magnetic field in the pipeline steel near the saturation flux density that interacts with anomalies to produce local changes (leakage) in this applied field close to the pipe's surface. Commonly, the pipeline materials (low-carbon steels) are soft-ferromagnetic alloys. The parameters of saturation (B_s or M_s), remanent magnetization (B_r or M_r) and coercivity (H_c) of these steels depend of the particular chemical composition, heat and rolling treatment, residual stresses, and density of inclusions.

A rule of thumb points that approximately three times the value of the steel coercivity (H_c) is needed to magnetize common low carbon steels for the purpose of magnetic testing. However, detailed research has found values for the magnetization that are outside of the typical value ranges. These typical values for industrial steels are: $B_s = 1.4$ -1.8 Tesla, $H_c = 3.5 - 20$ Oe, and $B_r = 0.3$ -1.5 Tesla.

To establish the magnetic field strength required to saturate the X52 and X70 steel samples, a magnetic properties test was run in the Electronics and Electrical Engineering Laboratory – Electromagnetic Division of the National Institute of Standards and Technology (NIST) in Boulder, CO. The longitudinal samples researched showed saturation magnetic flux density (B_s) at 1.8 Tesla (18,000 Gauss) and the radial or transverse samples at 1.6 Tesla (16,000 Gauss) (Figure 5.6). Notice that in the radial direction of the pipe the maximum saturation magnetic field density (B_{sR}) of both steels, X52 and X70, is slightly greater than in the longitudinal direction (B_{sL}), due to the rolling texturing obtained in the tested specimens. Moreover, the magnetic field required to saturate the steel in the radial direction (H_{sR}) is significantly lower to the field needed in the longitudinal direction (H_{sL}) of the pipe. B_{sR} is barely greater than B_{sL} probably because of the test specimen shape; while H_{sR} is considerably lower then H_{sL} because of the orientation of grains after hot rolling.

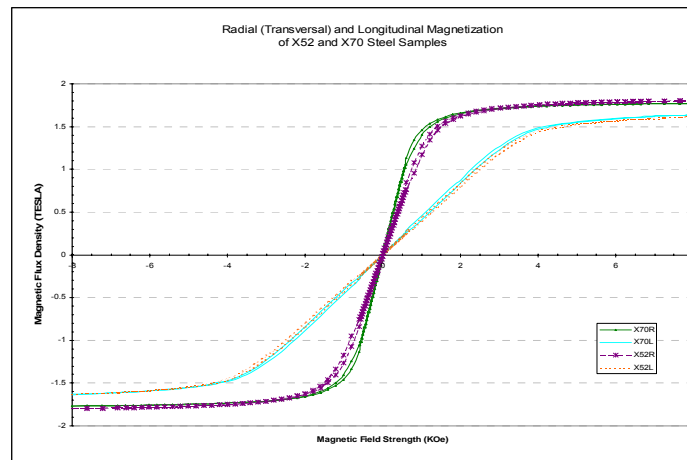


Figure 5.6. Magnetization Test results

Attachment # 3

References

REFERENCES

- American Petroleum Institute –API– Specification 5L: “Specification for Line Pipe”. Forty-Second Edition, 2000.
- American Society of Metals - ASM: “Corrosion: Fundamentals, Testing, and Protection.” Handbook Volume 13A, 2002.
- American Society of Metals - ASM: “Failure Analysis and Prevention.” Handbook Volume 11, 2002.
- AMT - Australian Magnet Technology PTY Ltd., History of Permanent Magnets, 2002. Web site: <http://www.magnet.au.com/magnet-history.html>.
- ASTM E1290-02: “Standard Test Method for Crack-Tip Opening Displacement (CTOD) Fracture Toughness Measurement.” American Society for Testing and Materials, 2002.
- ASTM F1113-99: “Standard Test Method for Electrochemical Measurement of Diffusible Hydrogen in Steels (Barnacle Electrodes).”
- ASTM G148-97: “ Standard Practice for Evaluation Uptaken, Permeation, and Transport in Metals by an Electrochemical Techniques.”
- Bhatia, A. and Westwood, S.: “ Developing a baseline in-line inspection program with design and operational decisions on the use of a high resolution magnetic flux leakage tool,” paper NACE No. 3172 presented at the NACE International Annual Conference and Exposition, 2003.
- Bickerstaff, R.; Vaughn, M.; Hassard, M.; and Garrett, M.: “Review of Sensor Technologies for In-Pipe Inspection of Natural Gas Pipeline.” Sandia National Laboratories, 2002, website: <http://www.netl.doe.gov/scng/publications/t&d/tsa/71702.pdf>.
- Bray, D.E. and Stanley, R.K., “Nondestructive Evaluation, a Tool in Design, Manufacturing, and Service.” Revised Edition. CRC Press, 1997.
- Bray, D.E. and McBride, D, “Nondestructive Testing Techniques.” New Dimensions in Engineering, John Wiley & Sons, Inc., 1992.
- Chikazumi, S., “Physics of Ferromagnetism.” The International Series of Monographs on Physics, Vol. 94, Second Edition. Oxford University Press, New York, 1997.
- Choe, S.B. and Shin, S.C.: “Calculations of the Surface Shape Anisotropy Induced at Rough Surfaces of Ferromagnetic Thin Films.” Journal of the Korean Physical Society, Vol. 38, No. 4, April 2001, pp. 392-395, website: http://cnsml.kaist.ac.kr/e_journal/jp392.pdf.
- Choumar, A.A.: “Pipeline Integrity Management through Intelligent Pigging Survey,” paper SPE-36275 presented at the 7th Abu Dhabi International Petroleum Exhibition and Conference of the Society of Petroleum Engineers, Abu Dhabi, U.E.A, 13-16 October 1996.
- Craig, B.D.: “Corrosion Product Analysis-A Road Map to Corrosion in Oil and Gas Production.” Material Performance Magazine, Volume 41, No.8, NACE, August 2002.
- Craig, B.D.: “Sour-Gas Design Considerations.” Society of Petroleum Engineers, Monograph Volume 15, Houston, 1993.
- Cramer, S.D. and Covino, B.S.: “Corrosion: Fundamentals, Testing, and Protection.” ASM Handbook Volume 13A, 2003.

- Crouch, A. E.: "In-Line Inspection of Natural Gas Pipelines." GRI-Report 91/0365, Gas Research Institute, 1992.
- Cullity, B. D., "Introduction to Magnetic Materials." Addison-Wesley Publishing Co., Inc., 1972.
- Das, K.B. et al: "Hydrogen embrittlement of Cathodically Protected 15-5PH Stainless Steel." Proceedings of the Second International Congress of Hydrogen in Metals, International Association of Hydrogen Energy, Volume 1-3E1, Paris, France, 6-10 June, 1977.
- DeLuccia, J.J., and Berman, D.A., "An Electrochemical technique to Measure Diffusible Hydrogen in Metals (Barnacle Electrode)." Electrochemical Corrosion Testing, eds. Mansfeld, F, and Bertocci, U. Philadelphia, PA: ASTM, 1981, p256.
- Devanathan, M.A.V. and Stachurski, Z, "The absorption and diffusion of electrolytic hydrogen in palladium." Proceedings of Royal Society, section A270, 1962, p90.
- Du Trémolet, E., Gignoux, D., and Schlenker, M., "Magnetism, I-Fundamentals." Klumer Academic Publishers, Norwell, 2002
- Elboujdaini M. *et al*: "Effects of Metallurgical Parameters and Non-Metallic Inclusions on Behaviour for Oil and Gas Industry Steels on Hydrogen Induced Cracking," paper No. 528, presented at 58th Annual Conference and Exposition of NACE, 2003.
- Flis, J. and Zakroczymski, T.: "Enhanced Hydrogen Entry in Iron at Low Anodic and Low Cathodic Polarizations in Neutral and Alkaline Solutions." Corrosion, NACE, p530-539, July 1992
- Fukai, Y. *et al*, "High Pressure Phase Diagram of Transition Metal-Hydrogen Systems." Department of Physics, Chuo University, Kasuga, Bonkyo-ku, Tokio, 2000. Website: <http://pfwww.kek.jp/acr2000/b/y00p202.pdf>.
- Garber, R. *et al*, "Effect of Carbon Content and Prior Austenitic Grain Size on Hydrogen Embrittlement of 1%Cr/0.75%Mo/0.025%Nb Steel in Aqueous Hydrogen Sulfide Environment." Proceedings of the Third International Conference on Effect of Hydrogen on Behavior of Materials, the Metallurgy Society of AIME, p361-377, Wyoming, 1980.
- Glicksman, M.E.: "Diffusion in Solids." John Wiley & Sons, Inc. NY, 2000.
- Hagiwara, N. and Meyer, M.: "Evaluating HSC of Line Pipe Steels under Cathodic Protection Using CTOD Tests," paper No. 380, presented at 55th Annual Conference and Exposition of NACE, 2000.
- Herve, J.L.; Udeli, J. and Ling M.T.S.: "New Techniques of Pipeline Inspection," paper SPE-10402. Society of Petroleum Engineers of AIME, 1981.
- Hirth, J.P.: "Effects of Hydrogen on the Properties of Iron and Steel." Metallurgical Transactions A, Vol. 11A, pp.861-890, 1980.
- Hodgman, R.Z., "Smart Pigging Philosophy," paper NACE No. 41 presented at the NACE International Annual Conference and Exposition, 1996.
- Huang, H. and Shaw, W.J.D., "Hydrogen Embrittlement Interactions in Cold-Worked Steel." NACE International, Corrosion – January 1995, Corrosion Science Section, p30.
- Interrante, C.G.: "Basic Aspects of the Problems of Hydrogen in Steels." Proceeding of the First International Conference of Current Solutions to Hydrogen Problems in Steels, p 3-17, American Society of Metals, Washington DC, 1982.

- Jiles, D., “ Introduction to Magnetism and Magnetic Materials.” Second Edition, Chapman and Hall, New York, 1998.
- Johnson, H.H. and Lin, R.W.: “Hydrogen and Deuterium Trapping in Iron.” Proceedings of the Third International Conference on Effect of Hydrogen on Behavior of Materials, the Metallurgy Society of AIME, p3-26, Wyoming, 1980.
- Jones, D.A.: “Principles and prevention of Corrosion,” 2nd Edition, Prentice Hall, NJ, 1996.
- Lauer, G. and Moreno P.: “New pigs combine previously separate detection technologies.” Pipe Line & Gas Industry Magazine, Vol. 84 No. 6, June 2001.
- MMC - Magnetic Materials and Components: “NEODYMIUM IRON BORON MAGNETS.” New York, 2001, website: http://www.mmcmagnetics.com/ourproducts/main_NdFeB.htm .
- Muhlbauer, K.: “Pipeline Risk Management Manual.” Gulf Publishing Company, Texas, 1992.
- Nave, C.R.: “ Hyperphysics.” Georgia State University, Department of Physics, 2002, website: <http://hyperphysics.phy-astr.gsu.edu/hbase/hframe.html>.
- Nye, B. and Garrison, C.: “Pigging Moves On-Improves Pipeline Safety and Operational Efficiency.” Pipeline & Gas Journal, August 2000.
- Nestleroth, J. B. and Bubenik, T. A., “Magnetic Flux Leakage (MFL) Technology For Natural Gas Pipeline Inspection.” The Gas Research Institute, 1999, website: <http://www.battelle.org/pipetechnology/MFL/MFL98Main.html#MeasurementVariables>.
- Nespeca, G.A., and Hveding, K.B.: “Intelligent Pigging of the Ekofisk-Emden 36-in. Gas Pipeline,” paper SPE-18232 presented at the 63rd Annual technical Conference and Exhibition of the Society of Petroleum Engineers, Houston, Texas, USA, October 2-5, 1988.
- Niyomsoan, S. *et al*: ‘The Relationship between Seebeck Coefficient and Phase Transformation of AB₂ Hydrogen Storage Materials,’ in progress. Colorado School of Mines, 2003.
- Olsen, S. *et al*: “Risk of Hydrogen Embrittlement from Cathodic Protection on Supermartensitic Stainless Steels,” paper No. 091, presented at 56th Annual Conference and Exposition of NACE, 2001.
- Oriani, R.A. *et al*: “Hydrogen Degradation of ferrous Alloys.” Noyes Publications, New Jersey, 1985.
- Pepperhoff, W. and Acet, M.: “Constitution and Magnetism of Iron and its Alloys.” Springer-Verlag, Engineering Materials. Berlin, 2001.
- Pressouyre, G.M.: “A Classification of Hydrogen Traps in Steels.” Metallurgy Transitions, Vol. 10A, p 1571-1573, 1979.
- Pigging Products and Services Association (PPSA): “An Introduction to Pipeline Pigging.” Gulf Publishing Company, Texas, 1995.
- Porter, P.C., “The application of new technology to the inspection of transmission and distribution pipelines,” paper NACE No. 43 presented at the NACE International Annual Conference and Exposition, 1996.
- Riecke, E. *et al*, “Influence of Microstructure of Iron and Steels on Steady State Hydrogen Permeation.” Proceedings of the Third International Conference on Effect

- of Hydrogen on Behavior of Materials, the Metallurgy Society of AIME, p97-104, Wyoming, 1980.
- Serna *et al*, “Effects of Wet Hydrogen Sulfide Environments on the Cracking Susceptibility of medium-Strength Microalloyed Pipeline Steels for Oil and Gas Transport,” paper No. 530, presented at 58th Annual Conference and Exposition of NACE, 2003.
 - Shamblin, T.R.: “Intelligent Pig Inspection of Uncoated Seamless Pipelines.” Pipeline & Gas Journal, March 2000.
 - Smith, S.N., Duvivier, J.P., Lefevre, D.E., and Robb, G.A.: “Field experiences with intelligent pigs,” paper NACE No. 37 presented at the NACE International Annual Conference and Exposition, 1996.
 - Staff Report: “Pigging - A good Year for Developments & Operational Success.” Pipeline & Gas Journal Online, August 2001.
 - Stevens, M.F. *et al*, “Analysis of Trapping Effects on Hydrogen Embrittlement of a HSLA Steel.” Proceedings of the Third International Conference on Effect of Hydrogen on Behavior of Materials, the Metallurgy Society of AIME, p341-348, Wyoming, 1980.
 - Talbot-Besnard, “Using Fundamental Studies to Find Possible Solutions to Hydrogen Problems in Steels.” Proceedings of the Third International Conference on Effect of Hydrogen on Behavior of Materials, the Metallurgy Society of AIME, p361-377, Wyoming, 1980.
 - Troiano, F., “Hydrogen Embrittlement and Stress Corrosion Cracking.” American Society of Metals, 1984.
 - Tuboscope: “Geometric Pigs Operation Principles.” Geometry Inspection, 2002, website: <http://www.tuboscopepipeline.com/docs/calgeoInsp.pdf>.
 - Vieth, P.H.: “Comprehensive, Long-Term Integrity Management Programs are being Developed and Implemented to reduce the Likelihood of Pipeline Failures.” Materials Performance Magazine, June 2002, pp. 17-22.
 - Van der Veer, P.A.J., Jager, S.F., Schmidt, R., and Bukman, F.: “Measuring Internal Corrosion in Small Diameter, Heavy Wall Pipelines.” Pipeline & Gas Journal, March 2000.
 - Vieth, P.H., Moghissi, O., and Beavers, J.A.: “Integrity-verification methods support US efforts in pipeline safety.” Oil and gas Journal, December 16, 2002, pp. 52-58
 - Yang, L., Fong, H., and Wong, Y.: “Research on intelligent pipeline magnetic flux leakage detector,” paper No. 11922 presented at 10th Asia-Pacific Conference on Non-Destructive Testing. Brisbane, Australia, 17-21 September 2001.
 - Yen, S.K. and Tsai, Y.C., “Critical Hydrogen Concentration for the Brittle Fracture of AISI 430 Stainless Steel.” Journal of Electrochemistry Society, Vol.143, No. 9, September 1996, p. 2736.
 - Yen, S.K., *et al*, “Effect of Electrolytic Zirconium Oxide Coating on Hydrogen Permeation of AISI 430 Stainless Steel.” NACE International, Corrosion – October 2000, Corrosion Science Section, p998.
 - Zhao, M.C., *et al*: “Role of Microstructure on Sulfide Stress Cracking of Oil and Gas Pipeline Steels.” Metallurgical and Materials Transactions, Volume 34A, p1089, May 2003.

Attachment # 4
Milestone Chart